nature

https://doi.org/10.1038/s41586-022-05273-0

Accelerated Article Preview

Dysregulated naïve B cells and de novo autoreactivity in severe COVID-19

Received: 10 August 2021

Accepted: 24 August 2022

Accelerated Article Preview

Cite this article as: Woodruff, M. C. et al. Dysregulated naïve B cells and de novo autoreactivity in severe COVID-19. *Nature* https://doi.org/10.1038/s41586-022-05273-0 (2022).

Matthew C. Woodruff, Richard P. Ramonell, Natalie S. Haddad, Fabliha A. Anam, Mark E. Rudolph, Tiffany A. Walker, Alexander D. Truong, Adviteeya N. Dixit, Jenny E. Han, Monica Cabrera-Mora, Martin C. Runnstrom, Regina Bugrovsky, Jennifer Hom, Erin C. Connolly, Igor Albizua, Vidhi Javia, Kevin S. Cashman, Doan C. Nguyen, Shuya Kyu, Ankur Singh Saini, Michael Piazza, Christopher M. Tipton, Arezou Khosroshahi, Greg Gibson, Greg S. Martin, Cheryl L. Maier, Annette Esper, Scott A. Jenks, F. Eun-Hyung Lee & Ignacio Sanz

Dysregulated naïve B cells and de novo autoreactivity in severe COVID-19

Authors: Matthew C. Woodruff[1,2], Richard P. Ramonell[3], Natalie S. Haddad[4], Fabliha A. Anam[1,2], Mark E. Rudolph[5], Tiffany A. Walker[6], Alexander D. Truong[7], Adviteeya N. Dixit[7], Jenny E. Han[6], Monica Cabrera-Mora[7], Martin C. Runnstrom[7], Regina Bugrovsky[1,2], Jennifer Hom[1,2], Erin C. Connolly[8], Igor Albizua[9], Vidhi Javia[7], Kevin S. Cashman[1,2], Doan C. Nguyen[7], Shuya Kyu[7], Ankur Singh Saini[1,2], Michael Piazza[10], Christopher M. Tipton[1,2], Arezou Khosroshahi[1,2], Greg Gibson[8], Greg S. Martin[7], Cheryl L. Maier[9], Annette Esper[7], Scott A. Jenks[1,2], F. Eun-Hyung Lee*[7], Ignacio Sanz*[1,2].

[1]Department of Medicine, Division of Rheumatology, Lowance Center for Human Immunology, Emory University, Atlanta, GA, USA

[2]Emory Autoimmunity Center of Excellence, Emory University, Atlanta, GA, USA

[3]Department of Medicine, Division of Pulmonary, Allergy and Critical Care Medicine, University of Pittsburgh, Pittsburgh, PA, USA

[4]MicroB-plex, Atlanta, GA, USA

[5]Exagen Inc., Vista, CA, USA

[6]Department of Medicine, Division of General Internal Medicine, Emory University, Atlanta, GA, USA

[7]Department of Medicine, Division of Pulmonary, Allergy, Critical Care and Sleep Medicine, Emory University, Atlanta, GA, USA

[8]School of Biological Sciences, Georgia Institute of Technology, Atlanta, GA, USA.

[9]Department of Pathology and Laboratory Medicine, Center for Transfusion and Cellular Therapies, Emory University School of Medicine, Emory University, Atlanta, GA, USA

[10]Nicoya, Kitchener-Waterloo, Canada

These authors contributed equally to this work: Matthew C. Woodruff and Richard P. Ramonell

*Corresponding Authors
F. Eun-Hyung Lee – F.E.Lee@emory.edu
Ignacio Sanz – Ignacio.sanz@emory.edu

Summary

Severe SARS-CoV-2 infection[1] has been associated with highly inflammatory immune activation since the earliest days of the COVID-19 pandemic[2-5]. More recently, these responses have been associated with the emergence of self-reactive antibodies with pathologic potential[6-10], although their origins and resolution have remained unclear[11]. Previously, we and others have identified extrafollicular B cell activation, a pathway associated with the formation of new autoreactive antibodies in chronic autoimmunity[12,13], as a dominant feature of severe/critical COVID-19[14-18]. Here, using single-cell B cell repertoire analysis of patients with mild and severe disease, we identify the expansion of a naïve-derived, low-mutation IgG1 population of antibody secreting cells (ASCs) reflecting features of low selective pressure. These features correlate with progressive, broad, clinically relevant autoreactivity, particularly directed against nuclear antigens and carbamylated proteins, emerging 10-15 days post symptom onset. Detailed analysis of the low selection compartment reveals a high frequency of clonotypes specific for both SARS-CoV-2 and autoantigens, including pathogenic autoantibodies against the glomerular basement membrane. We further identify the contraction of this pathway upon recovery, re-establishment of tolerance standards, and concomitant loss of acute-derived ASCs irrespective of antigen specificity. However, serological autoreactivity persists in a subset of patients with post-acute sequelae, raising important questions as to the contribution of emerging autoreactivity to ongoing symptomology upon recovery. In total, this study reveals the origins, breadth, and resolution of autoreactivity in severe COVID-19, with implications for early intervention and treatment of patients with post-COVID sequelae.

Main text

In 2019, the novel betacoronavirus SARS-CoV-2 emerged from Wuhan, China, resulting in the COVID-19 pandemic[1]. With reported mortality around 2 percent, early characterizations of severe disease emphasized the pro-inflammatory cytokine IL-6 and invoked the possibility of cytokine storms[2,3]. These observations, alongside observed efficacy of high-dose steroids in these patients were highly suggestive of immune responses not only responsible for viral clearance, but potentially contributing to disease pathology[4,5]. Profound alterations within the immune compartment were quickly identified as correlates of these inflammatory responses, with distinct patient immunotypes displaying increased frequencies of circulating plasmablasts yet lacked evidence of T follicular help (Tfh)[19]. This was bolstered by the identification of collapsed germinal center environments in patients that had succumbed to COVID-19[14].

Deep analysis of B cell activation pathways by our group and others has revealed strong emphasis of the extrafollicular (EF) pathway as a common feature of severe disease[14,15,17]. Characterized by the induction of Tbet-driven double negative 2 ($CD27^-$, IgD^-, $CD11c^+$, $CD21^-$ [DN2]) B cells, expansion of $CD19^+$ antibody secreting cells (ASCs), and depression of mutation frequencies within the ASC repertoire, these responses are highly similar to those we had identified previously in patients with active severe SLE[13,20]. In these patients, EF response activation results in the *de novo* generation of naive-derived autoreactivities despite the presence of chronic preformed autoimmune memory, and correlated with disease severity[12]. At the time of our study's publication, evidence of autoreactivity was mounting in severe disease, with observations of autoantibody-linked blood clotting[6], anti-interferon antibodies[7], connective tissue disease-associated interstitial lung disease (CTD-ILD)[8], and generalized observations of clinical autoreactivity[9], including our findings of expanded *IGHV4-34* B cells[15,21]. These observations have been bolstered by the reporting of broad autoreactivity within these patients – frequently targeting critical immune components[10], with serological kinetics strongly suggesting onset of new autoreactivity[11]. However, the developmental origins of these autoreactivities, their connection with the underlying *de novo* antiviral response, and their ultimate resolution remain unknown.

Viral-specific ASCs in severe COVID-19

Previous work established robust expansion of the ASC compartment as a hallmark of severe COVID-19[15,19]. Retrospective analysis of previously collected data from 25 (Healthy Donor (HD) = 9; Outpatient (OUT-C) = 7; ICU-patient (ICU-C) = 9) patients revealed that such expansion also includes the more mature CD19-negative ASC fraction we first reported to contain the long-lived plasma cells in the human bone marrow and has not been previously measured in COVID-19 infection or other acute immune responses in humans (Extended data 1a-c, Supplemental tables 1,2)[22]. Consistent with previous findings, ASC expansion in the ICU-C cohort was directly correlated with expansion of DN2 B cells, an important intermediate in the naïve-derived extrafollicular (EF) B cell response pathway (Extended data 1a,d)[13,15].

Although ASC expansion correlates with increased serological IgG responses to the SARS-CoV-2 spike protein receptor binding domain (RBD) in patients with severe disease[15], their direct contribution to that response has not been assessed. Using a novel *in vitro* method that optimizes overnight antibody secretion from PBMC-purified ASCs into the culture supernatant (media enriched in newly synthesized antibodies; MENSA[23]), ICU-C patients displayed higher frequencies of blood ASC secreting IgG RBD-specific antibodies confirming the relevance of early circulating ASCs to the antiviral response as opposed to non-specific cellular expansion (Fig 1a). Indeed, overall IgG-switched RBD-targeted MENSA titers were directly correlated with ASC expansion across the $COVID\text{-}19^+$ cohorts (Fig 1b).

Low selective pressure in expanded ASCs

In SLE, naïve-derived EF ASC expansions result in new autoreactive clones[12]. With considerable literature pointing to the presence of autoreactivity as a feature of severe COVID-19[6,7,10], it was important to understand the ASC contribution both to antiviral and autoantigen targeting. However, direct binding studies of these IgG^+ cells are hampered by their propensity to downregulate surface B cell receptor (BCR) in contrast to their IgM^+ counterparts (Fig 1c). Thus, antigen-specific flow-based study of this population would incompletely assess the ASC contribution to the overall antigen-specific response, and that broad analysis of this cellular compartment independent of BCR expression and antigen-specific probing was required.

To study the nature of the ASC compartment within these patients, 6 of 10 recruited ICU patients without dexamethasone treatment, alongside 4 patients with mild disease and 3 demographically matched healthy donors were selected for single cell VDJ repertoire (scVDJ) analysis. More than 17,000 ASCs were sequenced at acute infection time points between 4 and 18 days post symptom onset, reflecting almost 9,000 independent ASC clonotypes across all patients (Supplemental table 3). Clonality of the library was consistent with previous descriptions of oligoclonal ASC expansion[15], with up 13% of clonotypes representing more than 3% of the total repertoire (Supplemental table 3). Isotype analysis demonstrated a consistent expansion of IgG1 in the ICU-C cohort relative to the dominance of IgA found in steady-state HD in this study and previous publications[24] (Fig 1d, Extended data 2a,b). Concomitant IgM^+ expansions in some patients, alongside clonal connectivity between IgM and IgG1 ASCs in the ICU-C group suggested that the IgG1 compartment might reflect the newly-minted Ag-specific ASC pool (Extended data 2a,c). An intermediate phenotype was observed in the OUT-C group with IgG1 increases that did not reach statistical significance (Extended data 2b). Emphasis of IgG1 clonotypes was consistent with enrichment of total serological IgG1 in the ICU-C cohort, and retrospective analysis of published single cell transcriptomics data collected from bronchoalveolar lavage fluid (BALF) of 10 intubated patients which identified substantial IgG1 expression in the plasmablast population (Extended data 3)[25].

The expanded $IgG1^+$ ASC compartment of ICU-C patients was distinguished by reduced mutation frequency relative to OUT-C and HD controls (fig 1e,f). Notably, mutation reduction was largely concentrated on the IgG1 compartment with 10-70% of all IgG1 ASC expressing VH germline sequences and overall mutation frequencies significantly decreased in comparison to the rest of the class-switched ASC compartment (Figure 1e-g). Consistent with these observations, an analysis of the selective pressure on the antibody complementarity determining regions, as determined by Bayesian estimates of antigen-driven selection (BASELINe)[26], revealed selective reduction in the IgG1 in the ICU-C cohort versus other class-switched compartments (Fig 1h). In SLE, a bellwether of reduced selective pressure is the increased incorporation of autoreactivity-prone IgHV4-34 clonotypes into the antigen-selected CD27+ B cell compartment; often a result of naïve-derived EF B cell responses[12]. A similar phenomenon was reflected in the repertoire of the ICU-C cohort with increased frequency of IGHV4-34 positive cells emerging specifically within the $IgG1^+$ ASC compartment (Fig 1i) – aligning with our previous observations of increased IGHV4-34 serology within these patients[15].

<u>Uncoupled ASC and memory compartments</u>

To more deeply understand the origins and persistence of the low-mutation IgG1 ASC compartment, the contemporaneous CD27+ memory B cells were additionally sorted and analyzed in 3 surviving patients from the original ICU cohort (Supplementary table 3). Consistent with the expected properties of established memory B cells, class switched CD27+ cells were more polyclonal and displayed high levels of SHM[12] (Supplemental Table 3). In contrast to their matched ASC counterparts, IgG1-expressing memory clonotypes displayed increased selective pressures and decreased frequency of IgG1 clonotypes expressing unmutated BCRs (Extended data 4a-c).

Formal connectivity analysis between the IgG1 ASC compartment and contemporaneous memory in the ICU-C cohort showed low levels of clonal sharing in two of three patients without significant differences with steady-state healthy donors, who in the absence of known immune perturbation, are presumed to be devoid of ongoing memory activation (Extended data 4d). Moreover, in the two patients that displayed active connections between memory and ASC compartments, the connections were dominated by higher-mutation clonotypes (>1%) (Extended data 4e). Indeed, across the dataset, only 4 low mutation clonotypes were identified as shared between the emerging ASC and memory compartments. In all, our findings indicate uncoupling and separate selection pressures between the IgG1 ASC and memory B cell repertoires (Extended data 4a-c), and are consistent the emergence during acute severe infection of a memory-independent, newly generated ASC compartment with reduced selective pressure.

Clinical autoreactivity in COVID-19

The developing ASC response characteristics observed at both the cellular and repertoire level were highly similar to previous observations in patients with active SLE[12,15]. To understand if COVID-19 responses also correlated with autoreactivity, plasma collected from 27 ICU-C, 18 OUT-C, 20 SLE, and 14 HD was assessed through testing of more than 30 clinically-relevant autoantigens by Exagen, Inc. and analyzed for autoreactivity associated with connective tissue disorders. Broad tolerance breaks were identified across the ICU-C cohort against a variety of targets including rheumatoid factor (2/27), phospholipids (3/27), nuclear antigens (11/27), and glomerular basement membrane (2/27) (Table 1). Most ICU patients displayed at least positive test, with some patients displaying positive tests for up to 7 independent autoantigens (Fig 2a). Higher 'densities' of autoreactivity were significantly increased in ICU-C patients, with 3 or more autoreactivities being found exclusively in ICU-C patients (Extended data 5a, Fig 2a).

Autoreactivity screening identified significant emergence of two autoreactivities – anti-nuclear antigen (ANA) and anti-carbamylated protein responses (CarP) (Fig 2b,c). While ANAs are well characterized in clinical autoimmunity, they can also be present in up to 15% of healthy subjects at immunofluorescence titers <1:80[27]. In contrast, over 40% of the ICU-C cohort displayed ANA reactivities at titers greater than 1:160 (Table 1). Anti-CarP antibodies, associated with tissue damage in Rheumatoid Arthritis and SLE[28,29], were specific to the ICU-C cohort and present in over 40% of patients (Table 1, Fig 2c). Of interest, titers of a-CarP were directly correlated with the overall number of tolerance breaks across the cohort (Extended figure 5b, Fig 2d). Despite similarities in B cell activation profiles, other canonical reactivities associated with SLE such as Sm/RNP, Ro, La, and even dsDNA were universally negative (Table 1).

To understand specificity to COVID-19, 28 additional plasmas were assessed from ICU patients displaying acute respiratory distress syndrome (ARDS) as a result of confirmed bacterial pneumonia (Table 1). Importantly, the autoreactivity profiles of these patients were highly similar to patients with critical COVID-19 – strongly suggesting that the autoimmune phenomena described in COVID-19 to-date may be generalizable to other severe pulmonary infections (Fig 2e, Table 1). Identification of similar self-targets, particularly anti-CarP and anti-glomerular basement membrane (GBM) titers suggests that currently available clinical tests may be employed to identify these phenomena in real time across a host of human infectious diseases (Table 1).

To validate the ICU cohort, retrospective study of 52 independent critically ill patients who had received autoantibody testing as part of routine clinical care at the discretion of their treating physicians was undertaken. More than 50% of patients resulted at least one positive test, with ANAs as the most common autoreactive feature (a-CarP antibody testing was not performed) (Extended data 6). Within ICU patients, disease severity correlated with tolerance breaks – patients displaying the highest C-reactive protein levels (CRP; a surrogate of disease severity in COVID-19[30]) displayed both increased numbers and intensities of autoreactive tests (Fig 2f-h). While longitudinal testing for this cohort was limited, 7 patients were tested 2 weeks after the initial draw

with 3 of 7 testing positive for ANAs on initial assessment (Fig 2i). In alignment with published work describing building serological autoreactivity in immune-targeted autoantibodies[11], all three patients displayed stable or increasing ANA titers despite decreased CRP, suggesting building autoreactivity profiles beyond the resolution of biomarkers of clinical illness. Combining the datasets, and supplementing with an additional 50 ICU patient plasmas, a cross-sectional analysis of ANA reactivity as a function of the day post COVID-19 symptom onset revealed a clear and significant emergence of autoreactivity that can be identified between days 10 and 15 following symptomatic severe infection (Fig 2j,k).

Self-reactivity in antiviral response

In addition to autoimmune serologies and repertoire features of IgG1 ASC, the contribution of IgG1 to autoreactivity in ICU-C was also supported by the identification of IgG1-specific ANA reactivity in that cohort which could not be identified in IgG2 (Extended data 7a). To investigate this possibility, 2 patients (ICU-1 and ICU-2) were identified for individual clonotype assessment and monoclonal antibody production/testing. These patients were representative of the overall cohort, with low ASC mutation frequencies and high incorporation of autoreactive-prone *IGHV4-34* clonotypes (Extended data 7b,c). In patient ICU-1, low mutation ASCs displayed more connections to the CD27- B cell fraction than the memory compartment, and high levels of IgM ASC connectivity to IgG1 ASCs in both patients was suggestive of recent development (Extended data 7d,e).

Clonotypes were selected from this ASC compartment (54 and 53 clonotypes from ICU-1 and ICU-2, respectively) based on their inclusion of an IgG1 member, low mutation frequency (<1%), and presence in the ASC compartment, CD27- compartment, or both. In addition to all expanded clonotypes (> 5 members), all *IGHV4-34*-expressing members were included in the screening analysis.

mAbs were screened against multiple SARS-CoV-2 antigens including S1, RBD, NTD, S2, ORF-3, and nucleocapsid (Fig 3a)[31], with more than 65% showed binding to one of the tested target antigens (Fig 3a,b). Interestingly, despite similar frequencies in antiviral targeting, responses against nucleocapsid and the spike N-terminal domain differed between patients ICU-1 and ICU-2, suggesting potential differences in response microenvironment. Despite their naive origin and low (or absent) somatic hypermutation, many of the resulting antibodies displayed high affinity with KDs in the low nanomolar range (Supplemental Table 4). Top binders to spike and nucleocapsid displayed affinities of $KD = 2.82 \times 10^{-9}$ and $KD = 9.93 \times 10^{-10}$, respectively – in range of several published neutralizing antibodies[32]. (Fig 3a, Extended data 8). Of interest, *IGHV4-34*-expressing clones were generally viral-targeted (Fig 3a). Overall, these data confirm this compartment as enriched for antigen-specific ASCs contributing to the emerging antiviral response.

However, despite the dominance of SARS-CoV2-specific ASC, ~30% of the clones tested did not show clear specificity to the tested proteins, and many displayed low binding (Fig 3a). Combined with low selective pressures, it was important to understand if these antibodies also contained autoreactive potential. To this end, monoclonals were screened for ANA binding as an established method for broad human B cell autoreactivity assessment[33]. In accordance with the patient's ANA serum positivity, 16% of all 107 mabs displayed ANA reactivity, equally distributed between both patients (Fig 3c). Specific antigen targeting was heterogeneous, with individual reactivities identified against cytoplasmic, nuclear, membrane, cytoskeleton, and Golgi antigens (Extended data 9a). Further screening against the highly disease-specific GBM antigen revealed several positive hits in the patient with anti-GBM serum reactivity (ICU-1; 4/54 or 8%) with 3 of 4 also displaying antiviral affinity (Fig 3d). Binding to human naive B cells was also tested – a feature of *IGHV4-34* antibodies in SLE linked to reactivity against the naïve B cell surface[34,35]. Consistent with autoreactive potential against B cells and other Lupus antigens, 10 of 30 VH4-34 antibodies demonstrated B cell binding, with 4 of them displaying reactivity to SARS-CoV-2 antigens as confirmed through surface plasmon resonance (Fig 3a, Extended data 9b)[34].

In total, 65% (15/23) of monoclonals with identified autoreactivity displayed some affinity to a screened viral antigen – highly similar to the overall antiviral reactivity of the total antibody pool. Autoreactivity was independent of somatic hypermutation with more than half of identified self-targeted antibodies (14/23) displaying germline BCRs (Fig 3a). Cross-reactivity between self-antigens and the RBD (highly specific to SARS-CoV-2) further confirmed the naïve origins of these autoreactive responses, and heterogeneity of antiviral targets associated with self-reactivity strongly favor a model where relaxed selective pressure in the ASC compartment, rather than dominant molecular mimicry driven by a specific viral protein, is likely responsible for the emergence of autoreactivity observed in this cohort.

Uneven autoreactive recovery in COVID-19

To understand the evolution of the low-mutation ASC compartment upon acute disease resolution, patients ICU1-3 were recruited for follow-up between 6 and 10 months post-symptom onset (Supplemental table 3). All three patients showed a contraction of the overall IgG1 ASC compartment from the acute phase of disease, with two showing reductions of over 50% (Fig 4a,b), down to frequencies comparable to steady-state HD (Fig 1d). Importantly, out of over 900 independent IgG1 ASC clonotypes identified in the acute phase of disease, only 2 could be detected in the recovery phase in both memory and ASC compartments. None of the 107 characterized clones were persistent at recovery irrespective of antiviral targeting. IgG1 ASC mutation frequencies were increased at recovery to HD steady state levels (Fig 4c), and the nature of those mutations reflected a normalization of selective pressures at levels similar to other contemporaneous class-switched ASC compartments (Fig 4d). Renewed censoring of *IGHV4-34* clonotypes in the ASC compartment across all 3 patients, and reductions in *IGHV4-34*+ IgG antibodies in the plasma at recovery time points further confirmed the re-establishment of tolerance standards (Fig 4e,f).

However, despite universal signs of a return to 'normal' tolerance environments within the ASC compartment, the resolution of clinical autoreactivities was more complex. While two of three patients (ICU-1:2) showed evidence of resolving autoreactivity in the blood across multiple target antigens (including high titers of anti-GBM antibodies), one of the two appeared to increase reactivity against cardiolipin 7 months following disease onset (Extended data 10a-c). Further, patient ICU-3 displayed increased reactivity against both rheumatoid factor and CarP antigens at 10 months post symptom onset versus the acute phase of infection suggesting that in a subset of patients, clinical autoreactivity may persist well beyond the acute phase of infection (Extended data 10c). To assess this possibility, plasma from 40 ICU-recovered patients with no history of autoimmune disorders were collected from post-acute sequelae of COVID-19 (PASC) clinics and combined with existing cohorts of acute patients for cross-sectional longitudinal analysis. Consistent with individual patient reactivities, an early emergence of ANA reactivity was observed which persisted at significant, albeit tapering levels over the following year (Fig 4g). Of the 20 PASC patients available more than 100 days post symptom onset, 7 (35%) displayed ANA reactivity. Similarly, anti-CarP responses remained elevated albeit at decreased levels in a large fraction of patients (ICU-C 35%, PASC 25%) within the recovery phase of COVID-19 (Fig 4h), further stressing the need for continued follow up in these patients to understand the long-term implications of tolerance breaks on ongoing symptomology and chronic autoimmune manifestations.

Discussion

While several studies have detailed the presence of autoantibodies in COVID-19, their mechanisms of generation, chronic pathogenic potential, and eventual resolution remain to be understood. While new recent information has clearly documented the appearance of de novo serological autoreactivity in patients hospitalized with severe infection, the precise cellular source of such autoreactivity remains unidentified. Indeed, both the naive and memory B cell compartments of healthy subjects contain a large degree of

autoreactive/polyreactive cells which could be triggered to produce autoantibodies in the context of severe inflammation through a combination of antigen-specific and non-specific stimuli[33,36-38]. Here, we assign that phenomenon, at least in large part, to a transient naïve-derived ASC compartment through mechanisms that by and large involve antigen-mediated triggering. These cells, enriched in autoreactive potential, emerge during the acute phase of severe COVID-19 and regress gradually during the recovery phase in most, but not all patients. This compartment is characterized by a predominance of IgG1 ASCs expressing antibodies with low or absent somatic hypermutation distributed in a pattern consistent with low antigenic selection pressure. Emergence of this population is correlated with increased clinical autoreactivity against a variety of self-antigens, routinely including nuclear antigens and carbamylated proteins. Importantly, while the re-establishment of indicators of selective pressure within the ASC repertoire was consistent amongst all patients, the presence of autoantibodies in the serum persisted into the recovery phase in many patients experiencing ongoing symptoms well into the recovery phase of disease raising significant questions as to their contributions to post-acute sequelae.

The origins of autoreactivity in COVID-19 have been an important area of debate due to their prognostic potential. Early reporting of autoreactivity against type-I interferons in critically ill patients suggested that if these autoantibodies pre-dated the infection, they may help predict those at high risk[7]. Here, we demonstrate definitively that autoantibodies of substantial affinity can be generated, *de novo*, at the earliest phases of the humoral immune response. Indeed, the identification of RBD-specific clonotypes with germline BCR configurations and autoreactive targeting confirms that autoreactivity and antiviral targeting can be generated simultaneously in the robust EF responses identified in severe COVID-19. Thus, while preformed autoantibodies are likely to play an important role in specific aspects of infection severity, they are unlikely to account for the robust autoreactive phenotypes identified routinely in these patients. Instead, the current work establishes experimentally that the early emergence of isotype-switched autoreactivity is not a proxy for pre-existing autoreactive memory.

Although emphasized in COVID-19, autoreactivity following severe viral infection has been well documented in mice with multiple potential mechanisms proposed. Early work by Roosnek and Lanzavecchia described efficient non-cognate antigen presentation by autoreactive B cells as a mechanism for autoreactivity induction[39]. That model was invoked a decade later to explain the significant fraction of autoreactive clonotypes emerging from LCMV infection[40]. Molecular mimicry, an independent model of tolerance breakdown, has also been postulated as the source of autoreactivity in viral infection. Best described in rheumatic fever where anti-streptococcal antibodies cross-react with cardiac myosin, different types of molecular mimicry have been invoked across a variety of infectious diseases[41-45]. In SLE as well, it has been suggested that peptide homology between Epstein-Barr virus and ribonucleoproteins could lead to B cell epitope spreading and disease development[46]. Our experimental data do indeed demonstrate a degree of cross-reactivity between SARS-CoV2 antigens and a variety of self-antigens – an observation that would likely expand with more extensive testing against more comprehensive self-antigen arrays. However, specifically measuring the degree to which molecular mimicry accounts for such cross-reactivity would require extensive molecular and structural studies of multiple antigens and antigen-monoclonal antibody structures outside the scope of the current work. In strict sense, while molecular mimicry would require the sharing of a linear or conformational epitope between different antigens, cross-reactivity at large may be mediated by binding to separate antigens devoid of shared epitopes through separate parts of the antigen-binding site, a promiscuity that is enhanced by large and heavily charged CDR3 frequently enriched in autoreactive B cells.

While our experimental approach does not address these mechanisms directly, the identification of extensive ASC cross-reactivity between viral- and self- antigens suggests that the most robust manifestation of molecular mimicry – a specific pathogenic protein driving autoreactivity against a consensus self-antigen – may not be the primary driver the autoreactivity emerging in COVID-19. This postulate is consistent with the lack of

correlation between individual viral targets and specific self-antigens as autoreactivity can be identified in clones targeting all tested components of SARS-CoV-2. Further, the same broad autoantigens (naïve B cells, for example) can be targeted by antibodies with specificity to nucleocapsid, RBD, or can have no discernable affinity to the dominant viral antigens tested (Fig 3a). Instead, the data presented here are most consistent with a model by which the highly inflammatory milieu created by severe COVID-19 would promote the unopposed expansion of a positively-selected naïve compartment endowed with substantial germline encoded autoreactivity through the EF response pathway[12,47]. This scenario would result in the rapid conversion of autoreactive activated T-bet+ naïve B cells and their intermediary DN2 effectors into functional autoantibody-producing ASCs, a mechanism strongly driven by Th1-like cytokines prominently including IFN gamma, which is highly correlated with COVID-19 severity[15,48], as we and others have documented in acute SLE[12,13,49].

This model, in which the initially expanded autoreactivity would be enriched for self-reactivities not subject to strong central tolerance and readily present in the naïve compartment might help explain the enduring tolerance against some antigens, such as dsDNA and MPO, which would be abundant in the local milieu of severe COVID-19 due to strong neutrophil activation and NET formation[50]. This was also true of individual ANA antigens such as La, Sm, and Ro which are associated with SLE, but remained negative throughout acute infection. This profile would be consistent with broad expansion of the autoreactivity previously documented in human naïve B cells, which is enriched for ENA-negative ANA+ reactivity[33] and normally censored in the germinal center[51]. Accordingly, our studies highlight the immunological consequences of uncensored extrafollicular expansion of autoreactive naïve B cells in severe COVID-19 infection, and suggest that common, clinically testable autoreactivities including ANA and anti-CarP reactivity may be useful in identifying these phenomena in a variety of severe infectious diseases in real time[14]. The pathologic potential of individual reactivities that emerges in these patients remains to be established, however the generation of autoantibodies associated with autoimmune diseases with antibody-mediated pathology, including anti-CarP and GBM, strongly suggests a pathogenic role.

A critical finding in this study is the restoration of normal features in the IgG1 ASC compartment after recovery, including size contraction and increased levels of somatic mutation and selection pressure on a par with contemporaneous memory cells of the same subclass. These changes indicate a dynamic process of acute expansion of naïve-derived IgG1 ASCs enriched in autoreactivity that dominates during severe infection and subsequently subsides. However, despite clear resolution at the cellular level, kinetic analysis of autoreactive serology presents a more subtle picture with general declines in autoreactivity that nonetheless may persist at significant levels for several months. In some patients, such as ICU-3, autoreactivity may even increase post-infection; it will be important to know if these features are associated with the future emergence of chronic autoimmunity.

This mixed picture is consistent with established properties of the EF response – not only in the dominant generation of short-lived plasmablasts, but also in their less-appreciated potential to generate long-lived plasma cells and to contribute to memory responses[52]. Although the absence of acute phase clonotypes from IgG1 memory at recovery argues against robust memory incorporation, this finding is tempered by the necessarily restricted depth of repertoire tracking afforded by single cell analysis and the lack of direct examination of tissue-based memory and plasma cells. Hence, the combination of large correlative clinical studies and more extensive cellular studies will be required to understand whether acute relaxations of tolerance do indeed result in an increased susceptibility to chronic autoimmunity in a small subset of patients. These studies could help identify a therapeutic window wherein, as in autoimmunity, infectious disease treatment could be tailored to diminish the generation and survival of autoreactive B cells. Further, interfering with the maturation of autoreactive naive B cells using anti-BAFF or similar therapies[53], depletion of emerging pathogenic autoantibodies through anti-ASC agents[54] or strategies aimed to cycling the patient's IgG fraction[55] may improve recovery outcomes. This current study informs that important future work, characterizing the

immunologic underpinning of emerging primary autoreactivity in COVID-19 and identifying potential avenues for monitoring those responses, real-time, in a clinical setting.

References

1 Andersen, K. G., Rambaut, A., Lipkin, W. I., Holmes, E. C. & Garry, R. F. The proximal origin of SARS-CoV-2. *Nat Med* **26**, 450-452, doi:10.1038/s41591-020-0820-9 (2020).

2 Chen, X. *et al.* Detectable Serum Severe Acute Respiratory Syndrome Coronavirus 2 Viral Load (RNAemia) Is Closely Correlated With Drastically Elevated Interleukin 6 Level in Critically Ill Patients With Coronavirus Disease 2019. *Clin Infect Dis* **71**, 1937-1942, doi:10.1093/cid/ciaa449 (2020).***

3 Henderson, L. A. *et al.* On the Alert for Cytokine Storm: Immunopathology in COVID-19. *Arthritis Rheumatol* **72**, 1059-1063, doi:10.1002/art.41285 (2020).

4 Group, R. C. *et al.* Dexamethasone in Hospitalized Patients with Covid-19. *N Engl J Med* **384**, 693-704, doi:10.1056/NEJMoa2021436 (2021).

5 Cao, X. COVID-19: immunopathology and its implications for therapy. *Nat Rev Immunol* **20**, 269-270, doi:10.1038/s41577-020-0308-3 (2020).***

6 Zhang, Y. *et al.* Coagulopathy and Antiphospholipid Antibodies in Patients with Covid-19. *N Engl J Med* **382**, e38, doi:10.1056/NEJMc2007575 (2020).

7 Bastard, P. *et al.* Autoantibodies against type I IFNs in patients with life-threatening COVID-19. *Science* **370**, doi:10.1126/science.abd4585 (2020).

8 Gagiannis, D. *et al.* Clinical, Serological, and Histopathological Similarities Between Severe COVID-19 and Acute Exacerbation of Connective Tissue Disease-Associated Interstitial Lung Disease (CTD-ILD). *Front Immunol* **11**, 587517, doi:10.3389/fimmu.2020.587517 (2020).

9 Bowles, L. *et al.* Lupus Anticoagulant and Abnormal Coagulation Tests in Patients with Covid-19. *N Engl J Med* **383**, 288-290, doi:10.1056/NEJMc2013656 (2020).

10 Wang, E. Y. *et al.* Diverse functional autoantibodies in patients with COVID-19. *Nature*, doi:10.1038/s41586-021-03631-y (2021).

11 Chang, S. E. *et al.* New-onset IgG autoantibodies in hospitalized patients with COVID-19. *Nat Commun* **12**, 5417, doi:10.1038/s41467-021-25509-3 (2021).

12 Tipton, C. M. *et al.* Diversity, cellular origin and autoreactivity of antibody-secreting cell population expansions in acute systemic lupus erythematosus. *Nat Immunol* **16**, 755-765, doi:10.1038/ni.3175 (2015).

13 Jenks, S. A. *et al.* Distinct Effector B Cells Induced by Unregulated Toll-like Receptor 7 Contribute to Pathogenic Responses in Systemic Lupus Erythematosus. *Immunity* **49**, 725-739 e726, doi:10.1016/j.immuni.2018.08.015 (2018).

14 Kaneko, N. *et al.* Loss of Bcl-6-Expressing T Follicular Helper Cells and Germinal Centers in COVID-19. *Cell* **183**, 143-157 e113, doi:10.1016/j.cell.2020.08.025 (2020).

15 Woodruff, M. C. *et al.* Extrafollicular B cell responses correlate with neutralizing antibodies and morbidity in COVID-19. *Nat Immunol* **21**, 1506-1516, doi:10.1038/s41590-020-00814-z (2020).

16 Hoehn, K. B. *et al.* Cutting Edge: Distinct B Cell Repertoires Characterize Patients with Mild and Severe COVID-19. *J Immunol*, doi:10.4049/jimmunol.2100135 (2021).

17 Sosa-Hernandez, V. A. *et al.* B Cell Subsets as Severity-Associated Signatures in COVID-19 Patients. *Front Immunol* **11**, 611004, doi:10.3389/fimmu.2020.611004 (2020).

18 Nielsen, S. C. A. *et al.* Human B Cell Clonal Expansion and Convergent Antibody Responses to SARS-CoV-2. *Cell Host Microbe* **28**, 516-525 e515, doi:10.1016/j.chom.2020.09.002 (2020).

19 Mathew, D. *et al.* Deep immune profiling of COVID-19 patients reveals distinct immunotypes with therapeutic implications. *Science* **369**, doi:10.1126/science.abc8511 (2020).

20 Jenks, S. A., Cashman, K. S., Woodruff, M. C., Lee, F. E. & Sanz, I. Extrafollicular responses in humans and SLE. *Immunol Rev* **288**, 136-148, doi:10.1111/imr.12741 (2019).

21 Pugh-Bernard, A. E. *et al.* Regulation of inherently autoreactive VH4-34 B cells in the maintenance of human B cell tolerance. *J Clin Invest* **108**, 1061-1070, doi:10.1172/JCI12462 (2001).

22 Halliley, J. L. *et al.* Long-Lived Plasma Cells Are Contained within the CD19(-)CD38(hi)CD138(+) Subset in Human Bone Marrow. *Immunity* **43**, 132-145, doi:10.1016/j.immuni.2015.06.016 (2015).

23 Haddad, N. S. *et al.* Novel immunoassay for diagnosis of ongoing Clostridioides difficile infections using serum and medium enriched for newly synthesized antibodies (MENSA). *J Immunol Methods* **492**, 112932, doi:10.1016/j.jim.2020.112932 (2021).

24 Mei, H. E. *et al.* Blood-borne human plasma cells in steady state are derived from mucosal immune responses. *Blood* **113**, 2461-2469, doi:10.1182/blood-2008-04-153544 (2009).
25 Grant, R. A. *et al.* Circuits between infected macrophages and T cells in SARS-CoV-2 pneumonia. *Nature* **590**, 635-641, doi:10.1038/s41586-020-03148-w (2021).
26 Yaari, G., Uduman, M. & Kleinstein, S. H. Quantifying selection in high-throughput Immunoglobulin sequencing data sets. *Nucleic Acids Res* **40**, e134, doi:10.1093/nar/gks457 (2012).
27 Satoh, M. *et al.* Prevalence and sociodemographic correlates of antinuclear antibodies in the United States. *Arthritis Rheum* **64**, 2319-2327, doi:10.1002/art.34380 (2012).
28 Li, Y. *et al.* Antibodies against carbamylated vimentin exist in systemic lupus erythematosus and correlate with disease activity. *Lupus* **29**, 239-247, doi:10.1177/0961203319897127 (2020).
29 O'Neil, L. J. *et al.* Neutrophil-mediated carbamylation promotes articular damage in rheumatoid arthritis. *Sci Adv* **6**, doi:10.1126/sciadv.abd2688 (2020).
30 Luo, X. *et al.* Prognostic Value of C-Reactive Protein in Patients With Coronavirus 2019. *Clin Infect Dis* **71**, 2174-2179, doi:10.1093/cid/ciaa641 (2020).
31 Haddad, N. S. *et al.* One-Stop Serum Assay Identifies COVID-19 Disease Severity and Vaccination Responses. *Immunohorizons* **5**, 322-335, doi:10.4049/immunohorizons.2100011 (2021).
32 Cheng, L. *et al.* Impact of the N501Y substitution of SARS-CoV-2 Spike on neutralizing monoclonal antibodies targeting diverse epitopes. *Virol J* **18**, 87, doi:10.1186/s12985-021-01554-8 (2021).
33 Wardemann, H. *et al.* Predominant autoantibody production by early human B cell precursors. *Science* **301**, 1374-1377, doi:10.1126/science.1086907 (2003).
34 Richardson, C. *et al.* Molecular basis of 9G4 B cell autoreactivity in human systemic lupus erythematosus. *J Immunol* **191**, 4926-4939, doi:10.4049/jimmunol.1202263 (2013).
35 Cappione, A. J., Pugh-Bernard, A. E., Anolik, J. H. & Sanz, I. Lupus IgG VH4.34 antibodies bind to a 220-kDa glycoform of CD45/B220 on the surface of human B lymphocytes. *J Immunol* **172**, 4298-4307, doi:10.4049/jimmunol.172.7.4298 (2004).
36 Mietzner, B. *et al.* Autoreactive IgG memory antibodies in patients with systemic lupus erythematosus arise from nonreactive and polyreactive precursors. *Proc Natl Acad Sci U S A* **105**, 9727-9732, doi:10.1073/pnas.0803644105 (2008).
37 Quách, T. D. *et al.* Anergic responses characterize a large fraction of human autoreactive naive B cells expressing low levels of surface IgM. *J Immunol* **186**, 4640-4648, doi:10.4049/jimmunol.1001946 (2011).
38 Scheid, J. F. *et al.* Differential regulation of self-reactivity discriminates between IgG+ human circulating memory B cells and bone marrow plasma cells. *Proc Natl Acad Sci U S A* **108**, 18044-18048, doi:10.1073/pnas.1113395108 (2011).***
39 Roosnek, E. & Lanzavecchia, A. Efficient and selective presentation of antigen-antibody complexes by rheumatoid factor B cells. *J Exp Med* **173**, 487-489, doi:10.1084/jem.173.2.487 (1991).
40 Hunziker, L. *et al.* Hypergammaglobulinemia and autoantibody induction mechanisms in viral infections. *Nat Immunol* **4**, 343-349, doi:10.1038/ni911 (2003).
41 Zabriskie, J. B. Streptococcal cross-reactive antigens in relation to rheumatic fever. *Zentralbl Bakteriol Orig* **214**, 339-351 (1970).
42 Fujinami, R. S. & Oldstone, M. B. Amino acid homology between the encephalitogenic site of myelin basic protein and virus: mechanism for autoimmunity. *Science* **230**, 1043-1045, doi:10.1126/science.2414848 (1985).***
43 Kirvan, C. A., Swedo, S. E., Heuser, J. S. & Cunningham, M. W. Mimicry and autoantibody-mediated neuronal cell signaling in Sydenham chorea. *Nat Med* **9**, 914-920, doi:10.1038/nm892 (2003).***
44 Cunningham, M. W. Molecular Mimicry, Autoimmunity, and Infection: The Cross-Reactive Antigens of Group A Streptococci and their Sequelae. *Microbiol Spectr* **7**, doi:10.1128/microbiolspec.GPP3-0045-2018 (2019).***
45 Lans, T *et al*. Clonally expanded B cells in multiple sclerosis bind EBV EBNA1 and GlialCAM. *Nature*. 2022 Mar;603(7900):321-327. doi: 10.1038/s41586-022-04432-7. (2022).
46 Laurynenka, V *et al*. A High Prevalence of Anti-EBNA1 Heteroantibodies in Systemic Lupus Erythematosus (SLE) Supports Anti-EBNA1 as an Origin for SLE Autoantibodies. *Front Immunol*. 2022 Feb 17;13:830993. doi: 10.3389/fimmu.2022.830993. (2022).
47 Duty, J *et al*. Functional anergy in a subpopulation of naive B cells from healthy humans that express autoreactive immunoglobulin receptors. J Exp Med. 2009 Jan 16;206(1):139-51. doi:10.1084/jem.20080611. (2009).

48 Lucas, C. *et al.* Longitudinal analyses reveal immunological misfiring in severe COVID-19. *Nature* **584**, 463-469, doi:10.1038/s41586-020-2588-y (2020).
49 Zumaquero, E. *et al.* IFNgamma induces epigenetic programming of human T-bet(hi) B cells and promotes TLR7/8 and IL-21 induced differentiation. *Elife* **8**, doi:10.7554/eLife.41641 (2019).
50 Arcanjo, A. *et al.* The emerging role of neutrophil extracellular traps in severe acute respiratory syndrome coronavirus 2 (COVID-19). *Sci Rep* **10**, 19630, doi:10.1038/s41598-020-76781-0 (2020).
51 Tiller, T. *et al.* Autoreactivity in human IgG+ memory B cells. *Immunity* **26**, 205-213, doi:10.1016/j.immuni.2007.01.009 (2007).
52 Elsner, R. A. & Shlomchik, M. J. Germinal Center and Extrafollicular B Cell Responses in Vaccination, Immunity, and Autoimmunity. *Immunity* **53**, 1136-1150, doi:10.1016/j.immuni.2020.11.006 (2020).
53 Huang, W. *et al.* Belimumab promotes negative selection of activated autoreactive B cells in systemic lupus erythematosus patients. *JCI insight* **3**, doi:10.1172/jci.insight.122525 (2018).
54 Ostendorf, L. *et al.* Targeting CD38 with Daratumumab in Refractory Systemic Lupus Erythematosus. *N Engl J Med* **383**, 1149-1155, doi:10.1056/NEJMoa2023325 (2020).
55 Blumberg, L. J. *et al.* Blocking FcRn in humans reduces circulating IgG levels and inhibits IgG immune complex mediated immune responses. *Science Advances* **5**, eaax9586, doi:doi:10.1126/sciadv.aax9586 (2019).

Tables

Table 1 – Summary of positive autoreactive tests

Autoreactive Target	*HD (n = 14)*	*OUT (n = 18)*	*ICU (n = 27)*	*ICU-PASC (n = 40)*	*ARDS (n = 29)*	*SLE (n = 20)*
dsDNA	0	0	0	1 (3%)		18 (90%)
ANA titer	2 (14%)	1 (6%)	11 (41%)	16 (40%)	18 (62%)	20 (100%)
Sm	0	0	0	0	0	6 (30%)
Ro52	0	0	1 (4%)	0	1 (3%)	12 (60%)
Ro60	1 (7%)	0	0	0	0	13 (65%)
La	0	0	0	0	0	3 (15%)
Jo	0	0	0	0	0	0
RN	0	0	0	0	0	14 (70%)
Ribosomal Protein	0	0	0	1 (3%)	0	6 (30%)
RNA Pol 3 IgG	0	0	2 (7%)	4 (10%)	2 (7%)	8 (40%)
RF IgM	0	1 (6%)	2 (7%)	2 (5%)	4 (14%)	8 (40%)
RF IgA	0	0	0	0	2 (7%)	4 (20%)
Citulinated protein	0	0	1 (4%)	0	3 (10%)	3 (15%)
Prothrombin IgM	0	2 (11%)	4 (15%)	1 (3%)	0	4 (20%)
Prothrombin IgG	0	0	0	1 (3%)	0	7 (35%)
CL IgM	0	0	0	0	1 (3%)	0
CL IgA	0	0	0	0	2 (7%)	1 (5%)
CL IgG	0	2 (11%)	2 (7%)	1 (3%)	2 (7%)	1 (5%)
B2GP1 IgM	0	0	0	0	0	0
B2GP1 IgA	0	0	0	0	0	1 (5%)
B2GP1 IgG	0	1 (6%)	1 (4%)	2 (5%)	1 (3%)	3 (15%)
MPO	0	0	0	0	0	0
PR3	0	0	0	0	1 (3%)	0
ANCA	0	0	3 (11%)	4 (10%)	1 (3%)	12 (60%)
p70	0	0	0	0	1 (3%)	9 (45%)
Carbamylated Protein	0	0	11 (41%)	10 (25%)	11 (38%)	14 (70%)
GBM	0	0	2 (7%)	0	1 (3%)	0

Methods

Human participants

All research was approved by the Emory University Institutional Review Board (Emory IRB nos. IRB00058507, IRB00057983 and IRB00058271) and was performed in accordance with all relevant guidelines and

regulations. Written informed consent was obtained from all participants or, if they were unable to provide informed consent, from designated healthcare surrogates. Healthy individuals (n = 20) were recruited using promotional materials approved by the Emory University Institutional Review Board. Individuals with COVID-19 (n = 19) were recruited from Emory University Hospital, Emory University Hospital Midtown and Emory St. Joseph's Hospital (all Atlanta, USA). All non-healthy individuals were diagnosed with COVID-19 by PCR amplification of SARS-CoV-2 viral RNA obtained from nasopharyngeal or oropharyngeal swabs. Individuals with COVID-19 were included in the study if they were between 18 to 80 years of age, were not immunocompromised and had not been given oral or intravenous corticosteroids within the preceding 14 d. Peripheral blood was collected in either heparin sodium tubes (PBMCs) or serum tubes (serum; both BD Diagnostic Systems). Baseline individual demographics are included in Supplementary Table 1. Study data were collected and managed using REDCap electronic data capture tools hosted at Emory University.

Banked ARDS frozen patient plasma (n = 28) was obtained as previously described[56].

Peripheral blood mononuclear cell isolation and plasma collection

Peripheral blood samples were collected in heparin sodium tubes and processed within 6 h of collection. PBMCs were isolated by density gradient centrifugation at 1,000g for 10 min. Aliquots from the plasma layer were collected and stored at −80 °C until use. PBMCs were washed twice with RPMI at 500g for 5 min. Viability was assessed using trypan blue exclusion, and live cells were counted using an automated hemocytometer.

Flow cytometry

Isolated PBMCs (2 × 106) were centrifuged and resuspended in 75 µl FACS buffer (PBS + 2% FBS) and 5 µl Fc receptor block (BioLegend, no. 422302) for 5 min at room temperature. For samples stained with anti-IgG, it was observed that Fc block inappropriately interfered with staining, so a preincubation step of the anti-IgG alone for 5 min at 22 °C was added before the addition of the block. Next, 25 µl of antibody cocktail (Supplementary Table 3) was added (100 µl staining reaction), and samples were incubated for 20 min at 4 °C. Cells were washed in PBS, and resuspended in a PBS dilution of Zombie NIR fixable viability dye (BioLegend, no. 423106). Cells were washed and fixed at 0.8% paraformaldehyde (PFA) for 10 min at 22 °C in the dark before a final wash and resuspension for analysis.

Cells were analyzed on a Cytek Aurora flow cytometer using Cytek SpectroFlo software. Up to 3 × 106 cells were analyzed using FlowJo v10 (Treestar) software.

Analysis software

Computational analysis was carried out in R (v3.6.2; release 12 Dec 2019). Heat maps were generated using the pheatmap library (v1.0.12), with data pre-normalized (log-transformed z-scores calculated per feature) before plotting. Custom plotting, such as mutation frequency violin plots, was performed using the ggplot2 library for base analysis, and then post-processed in Adobe Illustrator. Alluvial plotting was performed using the ggalluvial package with post-processing in Adobe Illustrator. Clonotype connectivity analysis was carried out using the R-based 'vegan' package, and then visualized through 'pheatmap' before post-processing in Adobe Illustrator. Statistical analyses were performed directly in R, or in GraphPad Prism (v8.2.1).

Analyses on the single cell VDJ annotated sequences were performed using the Immcantation tool suite (http://www.immcantation.org) version 4.1.0 pipeline in Docker. This suite contains SHazaM for statistical analysis of somatic hypermutation (SHM) patterns as described in (Gupta et al., 2015), and BASELINe (Bayesian estimation of Antigen-driven SELectIoN) for analysis of selection pressure as described in (Yaari et al., 2012). Visualizations were generated in R using the SHazaM package (version 1.0.2) and then post-processed in Adobe Illustrator.

Flow cytometry and sorting of B cell subsets for repertoire sequencing

Frozen cell suspensions were thawed at 37 °C in RPMI + 10% FCS and then washed and resuspended in FACS buffer (PBS + 2% FCS). The cells were incubated with a mix of fluorophore-conjugated antibodies for 30 min on ice. The cells were washed in PBS and then incubated with the live/dead fixable aqua dead cell stain (Thermo Fisher) for 10 min at 22 °C. After a final wash in FACS buffer, the cells were resuspended in FACS buffer at 107 cells per ml for cell sorting on a three-laser BD FACS (BD Biosciences).

For single-cell analysis, total ASCs were gated as CD3−CD14−CD16−CD19+CD38+CD27+ single live cells, whereas naive B cells were gated as CD3−CD14−CD16−CD19+CD27−IgD+CD38+ single live cells.

For bulk sequencing preparations, B cells were enriched using StemCell's Human Pan-B Cell Enrichment Kit (no. 19554; negative selection of CD2, CD3, CD14, CD16, CD36, CD42b, CD56, CD66b and CD123). CD138+ ASCs were enriched further using CD138+ selection beads according to the manufacturer's instructions (Miltenyi Biotec, no. 130-051-301).

Single cell V(D)J repertoire library preparation and sequencing

Cells were counted immediately using a hemocytometer and adjusted to 1,000 cells per µl to capture 10,000 single cells per sample loaded in the 10× Genomics Chromium device according to the manufacturer's standard protocol (Chromium Next GEM Single Cell V(D)J Reagent Kits, v1.1). The 10× Genomics v2 libraries were prepared using the 10x Genomics Chromium Single Cell 5′ Library Construction Kit per the manufacturer's instructions. Libraries were sequenced on an Illumina NovaSeq (paired-end; 2 × 150 bp; read 1:26 cycles; i7 index: 8 cycles, i5 index: 0 cycles; read 2: 98 cycles) such that more than 70% saturation could be achieved with a sequence depth of 5,000 reads per cell.

Carbodiimide coupling of microspheres to SARS-CoV-2 antigens

Two SARS-CoV-2 proteins were coupled to MagPlex Microspheres of different regions (Luminex). Nucleocapsid (N) protein expressed from Escherichia coli (N-terminal His6) was obtained from Raybiotech (230-01104-100) and the RBD of spike (S) protein expressed from HEK293 cells was obtained from the laboratory of J. Wrammert63 at Emory University. Coupling was carried out at 22 °C following standard carbodiimide coupling procedures. Concentrations of coupled microspheres were confirmed by Bio-Rad T20 Cell Counter.

Luminex proteomic assays for measurement of anti-antigen antibody

Approximately 50 µl of coupled microsphere mix was added to each well of 96-well clear-bottom black polystyrene microplates (Greiner Bio-One) at a concentration of 1,000 microspheres per region per well. All wash steps and dilutions were accomplished using 1% BSA, 1× PBS assay buffer. Sera were assayed at 1:500 dilutions and surveyed for antibodies against N or RBD. After a 1-h incubation in the dark on a plate shaker at 800 r.p.m., wells were washed five times in 100 µl of assay buffer, using a BioTek 405 TS plate washer, then applied with 3 µg ml−1 PE-conjugated goat anti-human IgA, IgG and/or IgM (Southern Biotech). After 30 min of incubation at 800 r.p.m. in the dark, wells were washed three times in 100 µl of assay buffer, resuspended in 100 µl of assay buffer and analyzed using a Luminex FLEXMAP 3D instrument (Luminex) running xPONENT 4.3 software. MFI using combined or individual detection antibodies (anti-IgA, anti-IgG or anti-IgM) was measured using the Luminex xPONENT software. The background value of assay buffer was subtracted from each serum sample result to obtain MFI minus background (MFI-B; net MFI).

Statistical analysis

Statistical analysis was carried out using Prism (GraphPad). For each experiment, the type of statistical testing, summary statistics and levels of significance can be found in the figures and corresponding legends. All measurements displayed were taken from distinct samples.

High-Throughput Surface Plasmon Resonance

HT-SPR data was collected through single-cycle kinetic analysis against either SARS-CoV-2 nucleocapsid or spike trimer (S2P). Monoclonal antibodies were pre-screened for antigen binding through luminex-based multiplex binding assessment (above), and select antibodies were analyzed for binding affinity testing. All data was collected with 1:1 referencing collected in real time on a Nicoya Alto HT-SPR with 8 referenced channels running in parallel on carboxyl-coated sensors. Ligand binding/regeneration conditions for each antigen were as follows:

S2P – SARS-CoV-2 spike trimer was resuspended in tris acetate buffer, pH4.5, and immobilized onto an EDC/NHS-activated carboxyl sensor for 5 min at 50ug/ml. Regeneration of the sensor was performed using Glycine HCl, pH 2.5 for 1 min.

Nucleocapsid – SARS-CoV-2 nucleocapsid protein was resuspended in tris acetate buffer, pH6, and immobilized onto an EDC/NHS-activated carboxyl sensor for 5 min at 50ug/ml. Regeneration of the sensor was performed using Glycine HCl, pH 3 for 1 min.

All single-curve kinetics were performed with 5, 3-fold analyte dilutions with final concentrations between 222nM and 914pM. Analytes were run in PBST, with interactions collected at 25C.

B cell binding assay

2-3 million healthy donor PBMCs were incubated with 5ug of mAb at 40C for 30 min. The cells were washed with 30x volume FACS buffer (1xPBS, 2%FBS) and subsequently stained with Ab to CD3, CD19, CD27, IgD and IgG, as well as with Zombie NIR. Staining was completed with 0.8 % Paraformaldehyde for fixation. Flow Cytometry analysis was performed on CytoFLEX (BD Biosciences). Dead cells and doublets were excluded. The median fluorescence intensity (MFI) of mAb (IgG) was determined on naïve B cell population.

Monoclonal antibody selection and production

Monoclonal antibodies were selected for production from the single-cell repertoire data obtained from patient ICU-1. Individual cells were clustered into clonotypes, and then assessed for clonotype size, nucleotide mutation frequency, isotype, and connectivity between sorted populations. Through progressive filtering, clonotypes were selected that met the following criteria:

1. Contained at least one IgG1 member
2. Had at least one member with a mutation frequency of <1%
3. Had at least one member in the ASC compartment, the CD27- compartment, or contained members in both.

With those criteria met, all expanded clonotypes (>5 individual cells identified in the clonotype), and all *IGHV4-34*$^{+}$ members were selected for monoclonal antibody production and screening – 55 clonotypes in all. The most frequently repeated BCR sequence from each clonotype was provided to Genscript for antibody production on a standard IgG1 backbone.

Clinical autoreactivity testing

For autoimmune biomarker analysis frozen plasma was shipped on dry ice to Exagen, Inc. (Vista, California, USA) which has a clinical laboratory accredited by the College of American Pathologists (CAP) and certified under the Clinical Laboratory Improvement Amendments (CLIA). Thawed plasma was aliquoted and distributed for the following tests: anti-nuclear antibodies (ANA) were measured using enzyme-linked immunosorbent assays (ELISA) (QUANTA Lite; Inova Diagnostics) and indirect immunofluorescence (IFA) (NOVA Lite; Inova Diagnostics); anti-double-stranded DNA (dsDNA) antibodies were also measured by ELISA and were confirmed by IFA with Crithidia luciliae; extractable nuclear antigen autoantibodies (anti-Sm, anti-SS-B/La IgG, anti-Scl-70 IgG, anti-U1RNP IgG, anti-RNP70 IgG, anti-CENP IgG, anti-Jo-1 IgG, and anti-CCP IgG) as well as Rheumatoid Factor (RF) IgA and IgM were measured using the EliA test on the Phadia 250 platform (ThermoFisher Scientific); IgG, IgM, and IgA isotypes of anti-cardiolipin and anti-β2□glycoprotein, as well as anti-Ro52, anti-Ro60, anti-GBM, anti-PR3, and anti-MPO were measured using a chemiluminescence immunoassay (BIO-FLASH; Inova Diagnostics); anti-CarP, anti-RNA-pol-III, and the IgG and IgM isotypes of anti-PS/PT were measured by ELISA (QUANTA Lite; Inova Diagnostics), while C- and P-ANCA were measured by IFA (NOVA Lite; Inova Diagnostics). All assays were performed following the manufacturer's instructions.

BALF Plasma Cell Gene Expression

To assess the constant region gene expression in BALF-derived ASCs, data was retrospectively analyzed from the UCSC data browser available here: https://www.nupulmonary.org/covid-19-ms1. Briefly, these data are representative of 10 ICU patients whose BALF was collected within 48 hours of intubation, with total isolated cells sequenced using the 10x single cell transcriptomics platform. Patient information and full methods are available in the associated manuscript, Grant et. al. 2021.

MENSA Generation

Medium enriched for newly synthesized antibodies (MENSA) was generated by isolating, washing, and culturing ASC-containing peripheral blood mono-nuclear cells (PBMC) from blood using a modified procedure previously described (REF). PBMC were isolated by centrifugation (1,000 ×g; 10 min) using Lymphocyte Separation Media (Corning) and Leucosep tubes (Greiner Bio-One). Five washes with RPMI-1640 (Corning) were performed to remove serum immunoglobulins (800 xg; 5 min), with erythrocyte lysis (3 mL; 3 min) after the second wash and cell counting after the fourth. Harvested PBMCs were cultured at 106 cells/mL in R10 Medium (RPMI-1640, 10% Sigma FBS, 1% Gibco Antibiotic/Anti-mycotic) on a 12-well, sterile, tissue culture plate for 24 h at 37° C and 5% CO2. After incubation, the cell suspension was centrifuged (800 ×g; 5 min) and the supernatant (MENSA) was separated from the PBMC pellet, aliquoted and stored at -80°C for testing.

COVID-19 Multiplex Immunoassay

SARS-CoV-2 antigens were coupled to MagPlex Microspheres of spectrally distinct regions via carbodiimide coupling and tested against patient samples as previously described (2). Results were analyzed on a Luminex FLEXMAP 3D instrument running xPonent 4.3 software. Median fluorescent intensity (MFI) using combined or individual PE-conjugated detection antibodies (anti-IgA/anti-IgG/anti-IgM) was measured using the Luminex xPONENT software on Enhanced PMT setting. The background value of assay buffer or R10 media was subtracted from the serum/plasma or MENSA results, respectively, to obtain MFI minus background (net MFI). Serum and plasma samples were tested at 1:500 dilution and MENSA was tested undiluted.

Selection of Antigens

MENSA and Serum samples

Four recombinant SARS-CoV-2 Ags were used in this study. The N protein (catalog no. Z03480; expressed in Escherichia coli), the S1 domain (aa 16–685; catalog no. Z03485; expressed in HEK293 cells) of the spike protein, and the S1-RBD (catalog no. Z03483; expressed in HEK293 cells) were purchased from GenScript. The S1-NTD (aa 16–318) was custom synthesized by GenScript. Each protein was expressed with an N-terminal His6-tag to facilitate purification, >85% pure and appeared as a predominant single band on SDS-PAGE analysis.

Monoclonal Antibody testing

RBD (catalog no. Z03483; expressed in HEK293 cells) and Nucleocapsid protein (catalog no. Z03480; expressed in Escherichia coli), were purchased from GenScript (same as the first version). S1 (catalog no. S1N-C52H3; HEK293), S2 (catalog no. S2N-C52H5; HEK293) and S1 N-terminal domain (NTD; catalog no. S1D-C52H6; HEK293) were purchased from ACROBiosystems. The C-terminus sequence of ORF3a (Accession: QHD43417.1, amino acids 134-275 plus N-terminal His6-Tag) was sent to Genscript for custom protein expression in E. coli.

Data availability

All FCM and sequencing data presented here are publicly available in alignment with current requirements for public disclosure before peer review. All FCM data presented and analyzed in this manuscript (Fig. 1) are publicly available in the FlowRepository at http://flowrepository.org/id/FR-FCM-Z2XF/.

Methods References

56 Nirappil, F. J. *et al.* Characteristics and outcomes of HIV-1-infected patients with acute respiratory distress syndrome. *J Crit Care* **30**, 60-64, doi:10.1016/j.jcrc.2014.10.020 (2015).

End Notes

Acknowledgments

This work was supported by National Institutes of Health grants: UL TR000424 (Emory Library IT), U54-CA260563-01 Emory SeroNet (I.S., F.E.L.), U19-AI110483 Emory Autoimmunity Center of Excellence (I.S.), P01-AI125180-01 (I.S., F.E.L.), R37-AI049660 (I.S.), 1R01AI12125 (F.E.L.), 1U01AI141993 (F.E.L), T32-HL116271-07 (R.P.R.). Bill and Melinda Gates Foundation: INV-002351 (F.E.L.). Clinical autoreactivity testing was provided by Exagen, Inc.

We would like to thank S. Auld, W. Bender, L. Daniels, B. Staitieh, C. Swenson, and A. Truong for their expertise and support of our research. We would also like to thank the nurses, staff, and providers in the 71 ICU in Emory University Hospital Midtown and the 2E ICU in Emory Saint Joseph's Hospital. We would like to thank S. Rey, S. Demers, M. Hammons, A. Sace, and R. LaFon, and the Sanz/Lee clinical coordination and sample processing teams for aid in sample identification, collection, preparation and serological screening. Finally, we would acknowledge Dr. Luisa Morales-Nebreda for her guidance in use of previously published datasets.

Author contributions

MCW, RPR, SAJ, FEL, and IS conceived of and directed this study. MCW and RB performed flow cytometry, mAb and serum autoreactivity testing, and mAb affinity testing used in the study. MC-M and ASS performed single cell sorting and sequencing. RPR, NSH, and FAA performed serum and mAb screening against viral antigens. MCW, JH, ECC, MP, and CMT analyzed and compiled the resulting data. RPR, MCR, and AK conducted chart review and identified patient samples for study inclusion, and TAW, ADT, AND, JEH, IA, VJ, KSC, DCN, SK, GSM, CLM, and AE provided critical patient samples for the study. MER and MP oversaw critical collaborations for patient autoreactivity screening and mAb affinity testing, respectively. ECC and GG provided critical feedback and support in data analysis and interpretation. MCW and IS wrote the manuscript with all authors providing editorial support.

Competing Interest Statement

Dr. Lee is the founder of MicroB-plex, Inc and has research grants with Genentech. Dr. Mark Rudolph is employed by Exagen, Inc. Dr. Michael Piazza is employed by Nicoya.

Additional Information

Supplementary information is available for this paper.

Correspondence and requests for materials should be addressed to Dr. Ignacio Sanz at ignacio.sanz@emory.edu or Dr. F. Eun-Hyung Lee at F.E.Lee@emory.edu

Figure legends

Figure 1 – Expansion of low-selection IgG1 ASC compartment is a hallmark of severe COVID-19

(a,b) MENSA samples from OUT-C (n = 7) or ICU-C (n = 9) patients were analyzed for IgG reactivity against the SARS-CoV-2 receptor binding domain. **(a)** RBD-specific IgG antibody in MENSA samples collected from OUT-C and ICU-C patients. **(b)** Linear correlation of RBD-specific IgG antibody in MENSA samples vs. ASC frequency of B cell-derived cells in OUT-C and ICU-C patients. **(c)** IgG^+ and IgM^+ frequency of total SM or ASC populations from ICU-C cohort. **(d-i)** ASCs from HD (n = 3), OUT-C (n = 4), or ICU-C (n = 6) patient cohorts were sorted for single B cell repertoire sequencing and subsequent analysis. **(d)** Average ASC isotype compositions of HD, OUT-C, or ICU-C patients **(e)** Representative ASC mutation frequency distributions by isotype in patients HD-1, OUT-1, and ICU-1. **(f)** IGHV-gene nucleotide mutation frequencies of indicated ASC isotypes in HD, OUT-C, or ICU-C patients. **(g)** IGHV-gene nucleotide mutation frequencies of IgG1, versus other class-switched ASCs from indicated cohort. **(h)** BASELINe selection analysis of CDR selection in ICU-C ASCs, grouped by isotype. Bars represent 95% CI within the group. **(i)** $IGHV4\text{-}34^+$ ASC frequency in IgG1, versus other class-switched ASCs. **(a,c,g,i)** Statistical significance was determined using two-tailed t-testing between indicated groups. **(g,i)** Paired analyses. **(f)** Statistical significance was determined using ANOVA with Tukey's multiple-comparisons testing between all groups. **(a-l)** *$P \leq 0.05$; **$P \leq 0.01$; ***$P \leq 0.001$. **(a,c,f)** Summary statistics: mean ± standard deviation (s.d.). **(h)** Summary statistics: mean ± 95%CI

Figure 2 – Characterizing clinical autoreactivity profiles in COVID-19

(a-e) HD, OUT-C, ICU-C, and ARDS patient frozen plasma was tested against a variety of autoantigens in Exagen's clinical laboratory. **(a)** Frequency of total positive clinical tests across the HD, OUT-C, and ICU-C cohorts. **(b)** Distribution of anti-nuclear antigen titers across the HD, OUT-C, and ICU-C cohorts. **(c)** Distribution of anti-CarP titers across HD, OUT-C, and ICU-C cohorts. **(d)** Linear regression of anti-carbamylated protein titers vs. total number of patient autoreactive breaks across the ICU-C cohort. Patients

with positive anti-CarP titers are highlighted in red. **(e)** Frequency of anti-CarP responses, broken down by titer in HD, OUT-C, ICU-C, and bacterially-induced ARDS patient cohorts. **(f)** Frequency of anti-nuclear antigen titers in high vs. low CRP patients within the independent ICU cohort. **(g)** Frequency of rheumatoid factor positive tests in high vs. low CRP patients within the independent ICU cohort. **(h)** Frequency of anti-nuclear antigen and rheumatoid factor positive tests in high vs. low CRP patients within the independent ICU cohort. **(i)** 2-week follow up testing of 7 patients from the independent ICU cohort. C-reactive protein and anti-nuclear antigen titers are displayed. **(j,k)** IF ANA titers were assessed for the combined patient cohorts [3a,g], alongside an additional 50 ICU patients. (total n = 129). **(j)** ANA reactivity as a function of time post-symptom onset. Red line indicates loess regression with 95% CI. **(k)** Time point-binned assessment of IF ANA reactivity. **(b,c,k)** Statistical significance was determined using ANOVA with Tukey's multiple-comparisons testing between all groups. *P ≤ 0.05; **P ≤ 0.01; ***P ≤ 0.001.

Figure 3 – IgG1 clonotypes are both anti-viral and autoreactive

(a) Overview of clonotype (mAb) testing from patients ICU-1 and ICU-2 (total n = 107). Clonotypes were selected from the IgG1$^+$ low-selection compartment described in [Fig 1,2]. (*Left*) Heatmaps of mAb (rows) binding to indicated antigens (columns). (*Middle*) KD – antibody affinities confirmed through HT-SPR; IGHV4-34 – Clonotype encodes IGHV4-34 receptor; Germline – Clonotype displays germline heavy and light chain configurations; Autoreactive – Clonotype displays autoreactivity against indicated autoantigen. (*Right*) Ab designation to aid tracking throughout [Fig 4] **(b)** SARS-CoV-2 antigen targeting across all 107 mAbs. **(c)** Mean fluorescence intensity (MFI) measurements of Hep2 cell line reactivity by synthesized monoclonals via immunofluorescence. Select mAb designations indicated [Fig 4a] **(e)** Anti-GBM ELISA testing of isolated monoclonal antibodies. Select clonotype designations indicated [Fig 4a]. **(c,d)** Summary statistics: Mean negative test value ± 3 standard deviations.

Figure 4 – Relaxed peripheral tolerance resolves in the repertoire upon recovery.

(a) Average isotype frequencies at acute and recovery time points from ICU-C patient cohort (6-10mo DPSO, n = 3) **(b)** IgG1 ASC isotype frequency in acute or recovery ICU-C cohort. **(c)** *IGHV* nucleotide mutation frequency in IgG1 ASCs in acute vs recovery samples in ICU-C cohort. **(d)** ASC selective pressure comparisons of selected isotypes from acute or recovery ICU-C cohort. Bars represent 95% CI within the group. **(e)** *IGHV4-34*$^+$ ASC frequency in IgG1 ASCs in acute vs recovery samples in acute or recovery ICU-C cohort. **(f)** ELISA assessment of *IGHV4-34*$^+$ IgG plasma antibody concentration in acute or recovery ICU-C cohort. (n = 4) **(g)** IF ANA titers were assessed for the combined acute patient cohorts [2j], alongside 45 ICU patients at recovery time points indicated. (total n = 174)**.** ANA reactivity is assessed as a function of time post-symptom onset. Red line indicates loess regression with 95% CI. **(h)** Frequency of anti-CarP positive reactivity in acute (n = 27) versus recovery (n = 40) ICU-C cohorts. **(b,c,e,f)** Statistical significance was determined using paired two-tailed t-testing between indicated groups. *P ≤ 0.05; **P ≤ 0.01.

Extended Data Legends

Extended data 1 – EF B cell activation in COVID-19

(a-d) PBMCs were isolated from HD (n = 9), OUT-C (n = 7), or ICU-C (n = 10) patients and analyzed by spectral flow cytometry. **(a)** Progressive gating strategy for flow cytometry. Label above plot indicated pre-gating population from previous plot. **(b)** CD19$^-$ ASC frequency of total ASCs. **(c)** ASC frequency of total B cell-derived cells. **(d)** Linear regression analysis of log2-transformed DN2 vs ASC frequencies of total B cell-derived cells. **(b,c)** Statistical significance was determined using ANOVA with Tukey's multiple-comparisons testing between all groups. *P ≤ 0.05; **P ≤ 0.01; ***P ≤ 0.001.

Extended data 2 – IgM-connected IgG1 ASC expansion in severe/critical COVID-19

(a-c) ASCs from HD (n = 3), OUT-C (n = 4), or ICU-C (n = 6) patient cohorts were sorted for single B cell repertoire sequencing and subsequent analysis. **(a)** Isotype frequencies of individual patients within the ICU-C, OUT-C, and HD cohorts **(b)** ASC subclass frequencies by indicated isotype in HD, OUT-C, and ICU-C cohorts. **(c)** Clonotype connectivity between IgM and IgG1 ASCs in HD, OUT-C and ICU-C cohorts. **(b,c)** Statistical significance was determined using ANOVA with Tukey's multiple-comparisons testing between all groups. *P ≤ 0.05; **P ≤ 0.01; ***P ≤ 0.001.

Extended data 3 – IgG1 ASCs are present in the BAL

(a) Statistical significance was determined using ANOVA with Tukey's multiple-comparisons testing between all groups. *P ≤ 0.05; **P ≤ 0.01; ***P ≤ 0.001. **(a)** Bulk IgG1 assessment in HD, OUT-C, or ICU-C cohorts. **(b)** Gene expression of indicated constant region in ASCs identified in the bronchoalveolar fluid from 10 ICU patients. Retrospective analysis of data collected by Grant et. al.

Extended data 4 – Low-mutation IgG1 ASCs are uncoupled from the contemporaneous memory

(a-e) Single cell VDJ analysis of ASCs and memory compartments from ICU-C patients (n = 3) **(a,b)** BASELINe selection analysis of CDR selection in ASC vs. memory B cell populations, grouped by isotype (n = 4). **(b)** Statistical selective pressure comparisons of selected isotypes. Bars = 95% CI **(c)** Frequency of clonotypes whose most expanded member maintains germline heavy and light chain BCR configuration from $IgG1^+$ ASC or $CD27^+$ memory compartments. **(d)** Clonotype connectivity between $IgG1^+$ ASCs and the contemporaneous $CD27^+$ memory compartment. Patients displaying any connectivity highlighted in green. **(e)** Relative clonal connectivity between mutated (>=1% mutation) versus unmutated (<1%) $IgG1^+$ ASCs and the contemporaneous memory. Only two patients showing active connection between the compartments [2d] are evaluated. **(c)** Statistical significance was determined using paired two-tailed t-testing between indicated groups. *P ≤ 0.05; **P ≤ 0.01.

Extended data 5 – Severe COVID-19 correlates with increased autoreactivity against multiple autoantigens

(a,b) HD, OUT-C, and ICU-C patient frozen plasma was tested against a variety of autoantigens in Exagen's clinical laboratory. **(a)** Distribution of total positive clinical tests across the HD, OUT-C, and ICU-C cohorts. **(b)** Linear regression of anti-carbamylated protein titers vs. anti-nuclear antigen titers across the ICU-C cohort. Patients with positive anti-CarP titers are highlighted in red.

Extended data 6 – Autoreactivity against clinical autoantigens correlates with inflammation

Heatmap display of Emory pathology-confirmed clinical results of 52 SARS-CoV-2 ICU patients with US NIH "severe" or "critical" clinical designations. Patients are organized by ascending CRP values (range 16.5-472.7). Individual testing scale values are indicated following the test name.

Extended data 7 – Phenotypes of patients selected for antibody screening

(a) ANA ELISA testing of 5 ICU-C patients with positive clinical testing as determined by Exagen, Inc. [Fig2a]. ELISAs were developed with isotype specific IgG1 and IgG2 secondary probes. Red dots indicate positive tests **(b)** Mutation frequency distributions of ICU-1 and ICU-2 ASC and $CD27^+$ memory compartments of indicated isotypes. **(c)** Frequency of autoreactivity-mediating 'AVY' patch integrity in IgG1 ASCs versus IgG1 memory in patients ICU-1 and ICU-2. **(d)** Alluvial plots showing clonotype connectivity between IgG1 ASCs to the $CD27^-$ or memory compartments. Individual clonotypes represented by vertical banding, with the height of the band reflective by the number of cells incorporated into the clonotype. Clonotypes with minimum mutation frequencies <= 1% are highlighted in green. **(e)** Alluvial plots showing clonotype connectivity between IgG1 ASCs to the IgM ASC compartment. Clonotypes with minimum mutation frequencies <= 1% are highlighted in green.

Extended data 8 – SPR-based affinity testing of naïve-derived, low mutation monoclonal antibodies

Representative raw data (blue), and model fitting (black) are displayed for each of the 5 antibodies tested for affinity via HT-SPR. Summary table displays the target, on rate (Ka), off rate (Kd), and affinity (KD), with associated standard deviations in parentheses.

Extended data 9 – Autoantigen reactivity screening of naïve-derived, low mutation monoclonal antibodies

(a) Representative staining patterns from select mAbs with reactivity against the Hep2 cell line as identified in [Fig 2c]. Select clonotype designations indicated [Fig 2a] **(b)** Naive B cell binding of two monoclonal antibodies as identified in [Fig 2a].

Extended data 10 – Longitudinal clinical autoreactivity profiles of patients ICU1-3

(a-c) Samples obtained at all time points from patients ICU-1:3 were sent to Exagen, Inc. for broad autoreactivity testing in their clinical laboratory. All clinical positive tests for each patient are displayed. Red dots indicate a positive clinical value. **(a)** Clinical positive tests for patient ICU-1 at indicated time points. **(b)** Clinical positive tests for patient ICU-2 at indicated time points. **(c)** Clinical positive tests for patient ICU-3 at indicated time points.

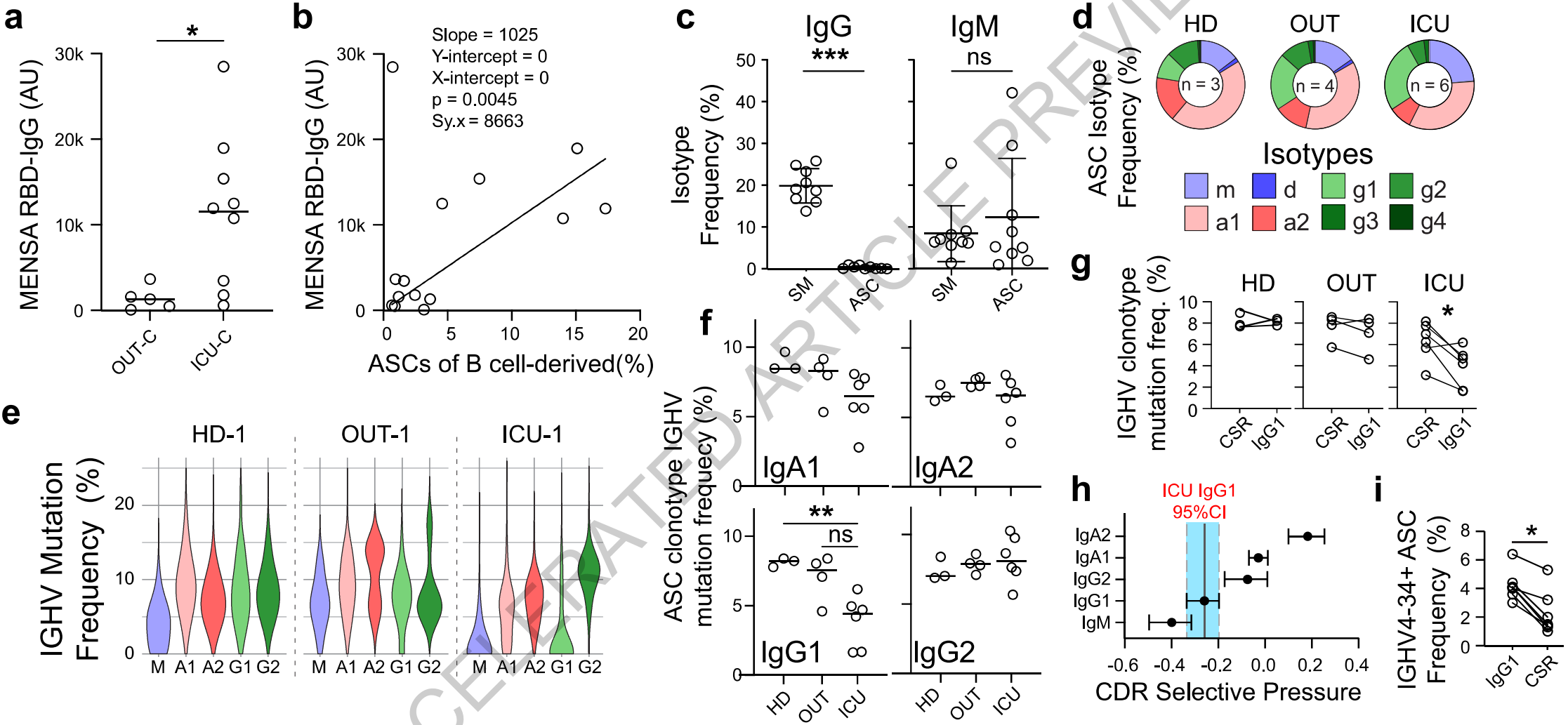

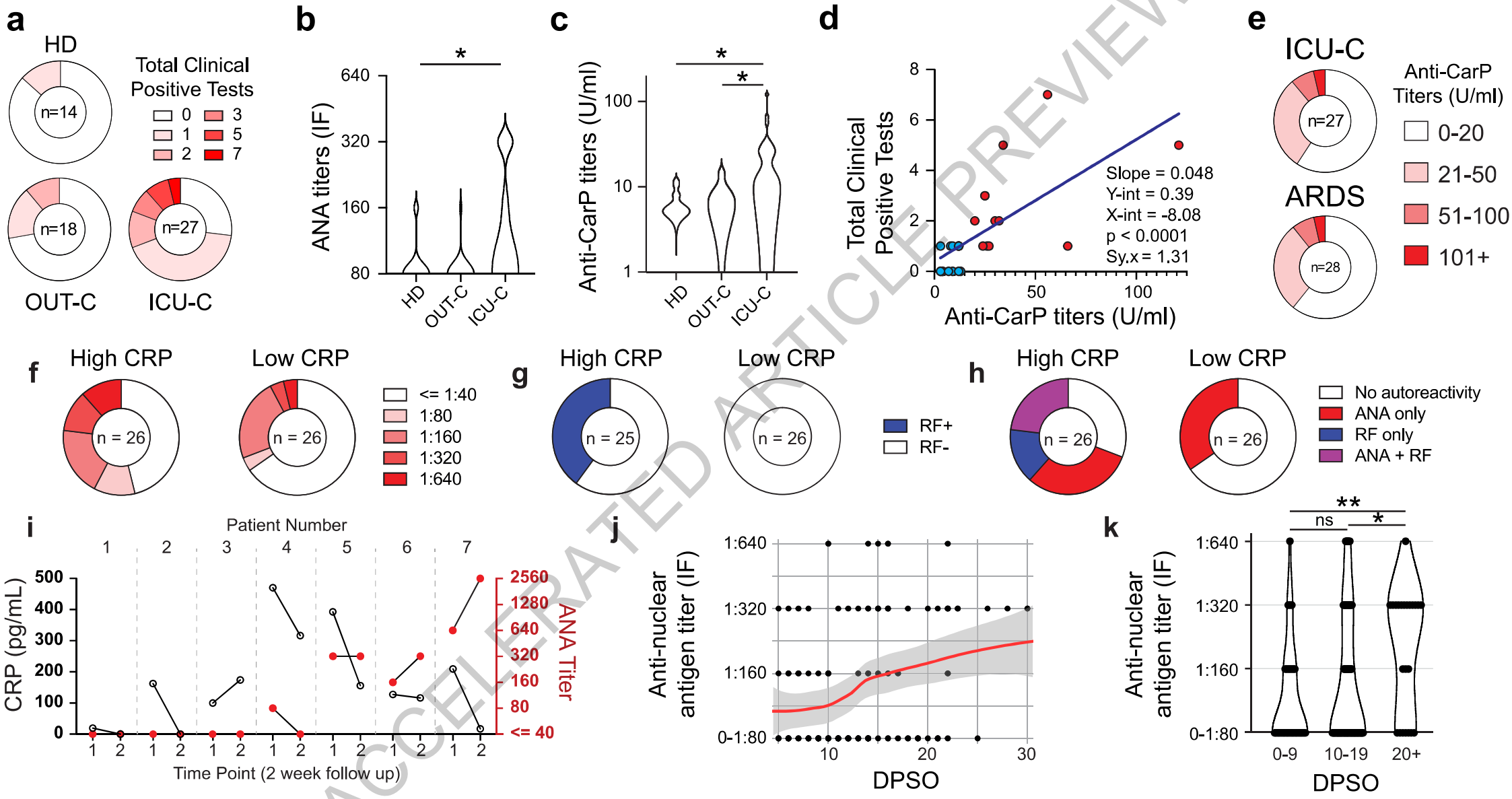

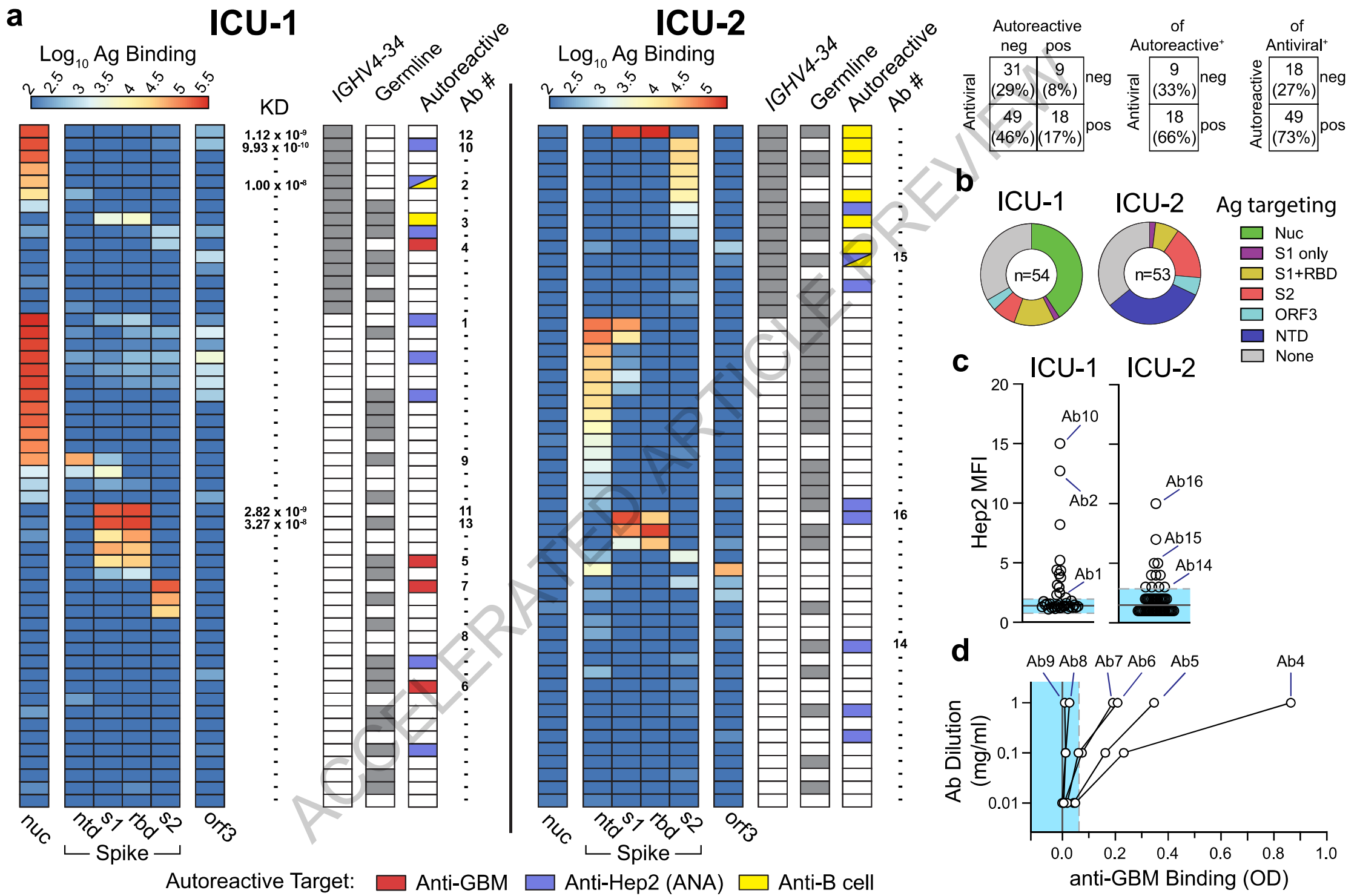
a
ICU-1
ICU-2
Log10 Ag Binding
2 2.5 3 3.5 4 4.5 5 5.5
KD
IGHV4-34
Germline
Autoreactive
Ab #
1.12 x 10-9
9.93 x 10-10
1.00 x 10-8
2.82 x 10-9
3.27 x 10-8
12
10
2
3
4
15
1
9
11
13
16
5
7
8
14
6
nuc
ntd
s1
rbd
s2
orf3
Spike
Autoreactive Target:
Anti-GBM
Anti-Hep2 (ANA)
Anti-B cell
Autoreactive
neg
pos
Antiviral
31 (29%)
9 (8%)
49 (46%)
18 (17%)
of Autoreactive+
9 (33%)
18 (66%)
of Antiviral+
Autoreactive
18 (27%)
49 (73%)
b
ICU-1
ICU-2
n=54
n=53
Ag targeting
Nuc
S1 only
S1+RBD
S2
ORF3
NTD
None
c
Hep2 MFI
Ab10
Ab2
Ab1
Ab16
Ab15
Ab14
d
Ab9 Ab8 Ab7 Ab6 Ab5 Ab4
Ab Dilution (mg/ml)
anti-GBM Binding (OD)
ACCELERATED ARTICLE PREVIEW

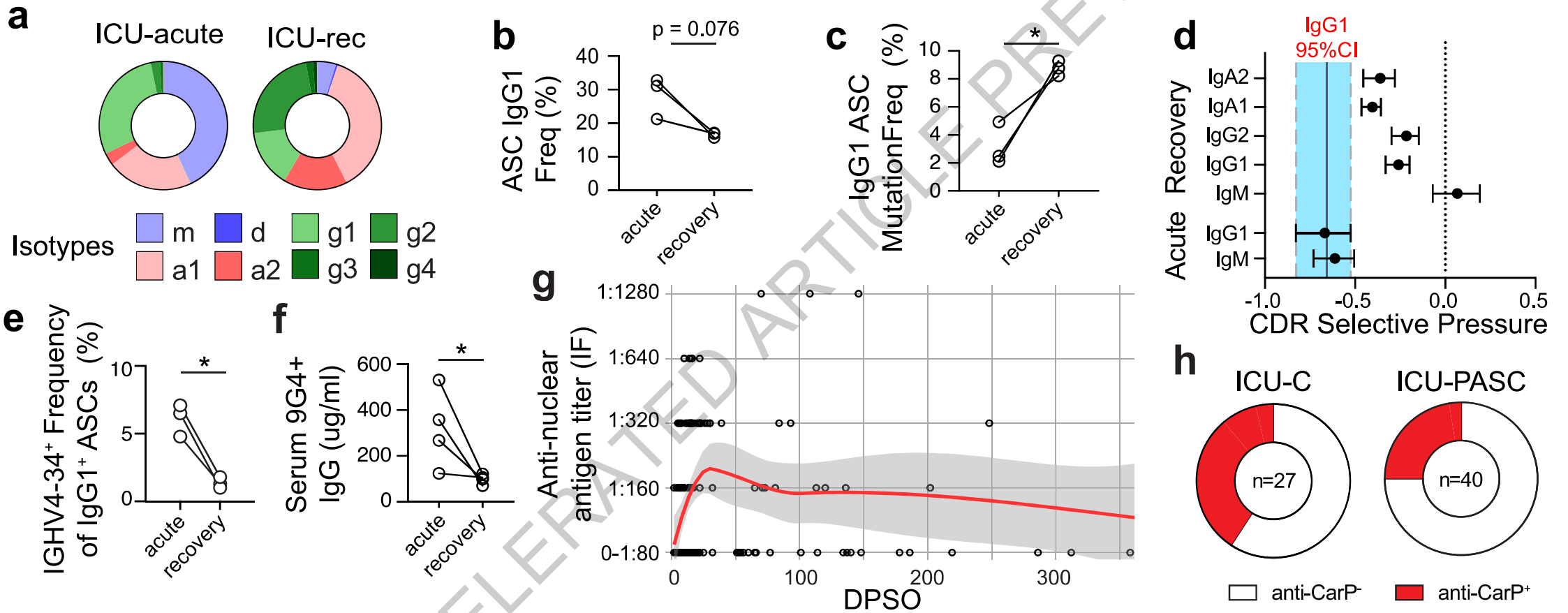

Extended data 1

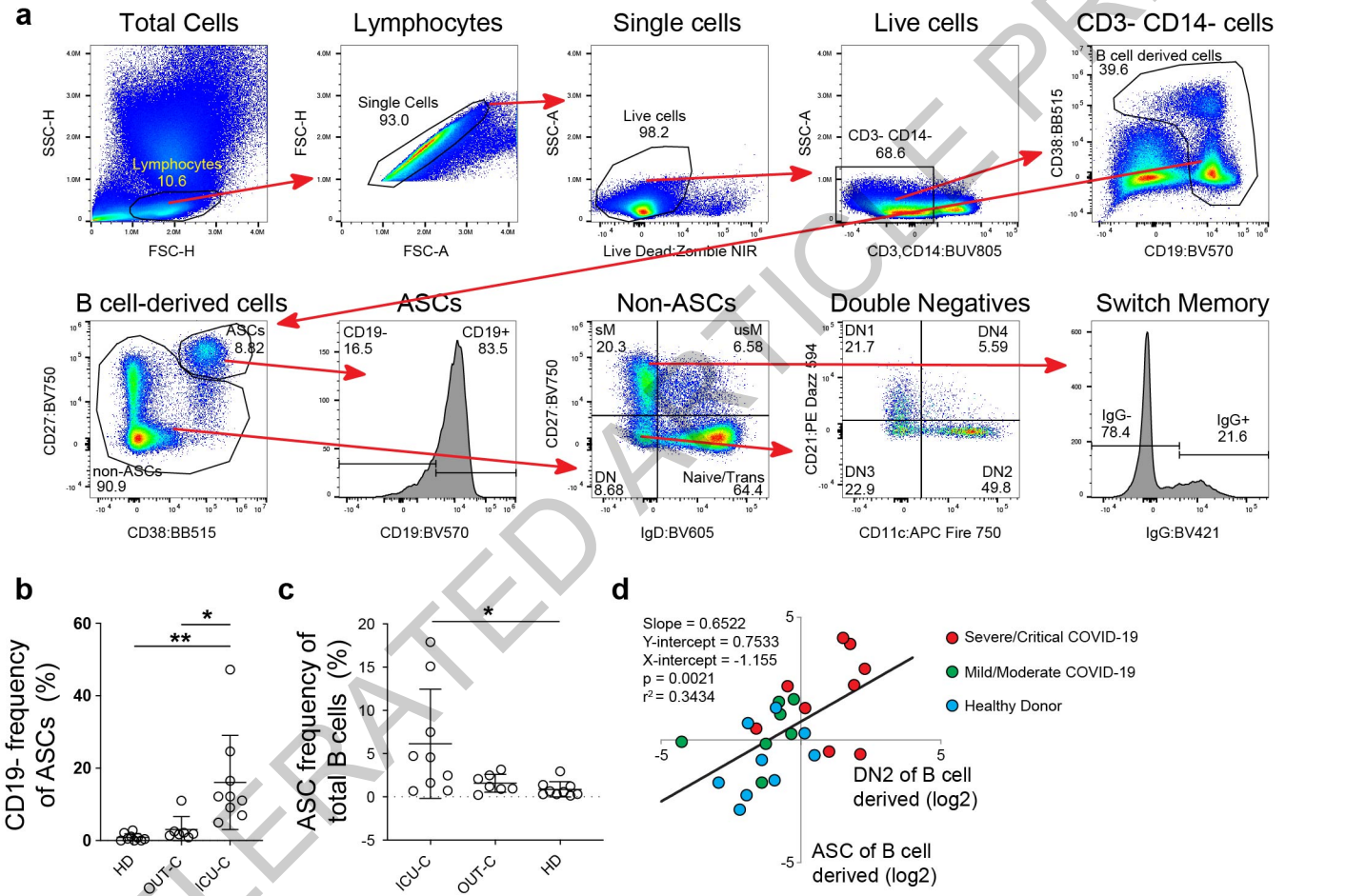

Extended data 2

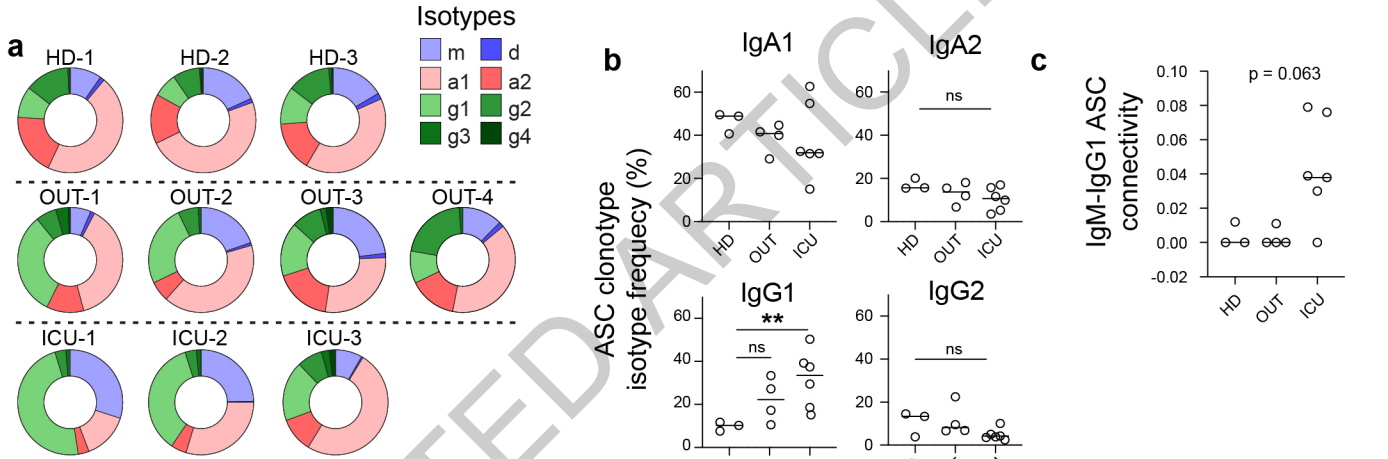

Extended data 3

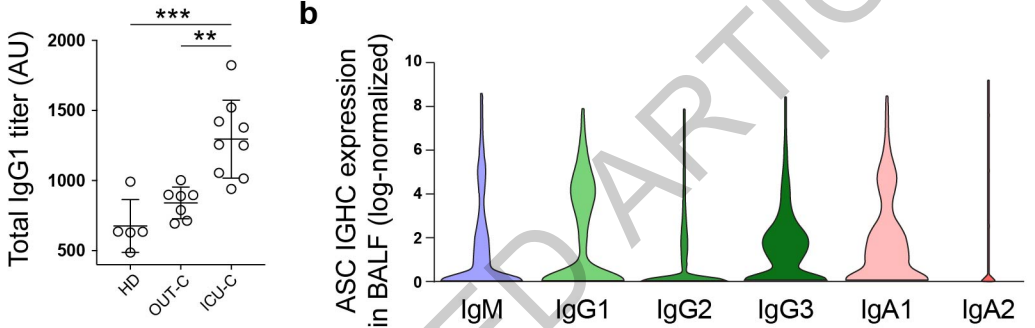

Extended data 4

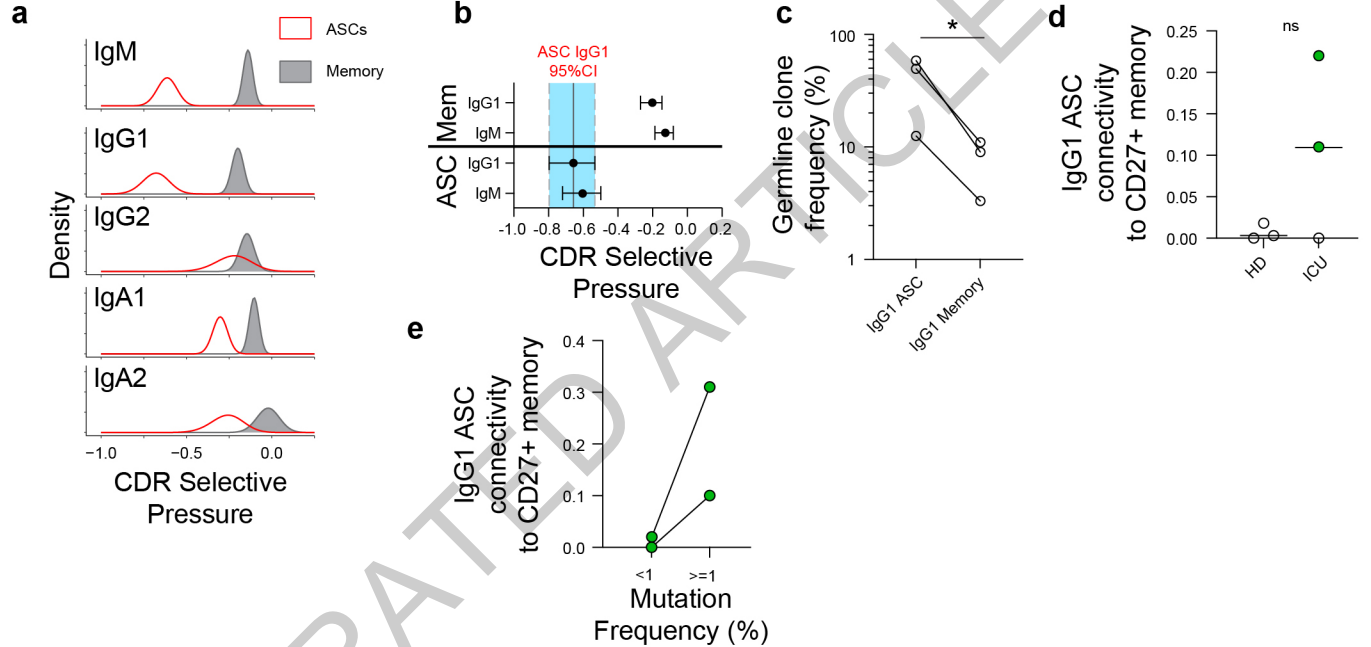

Extended data 5

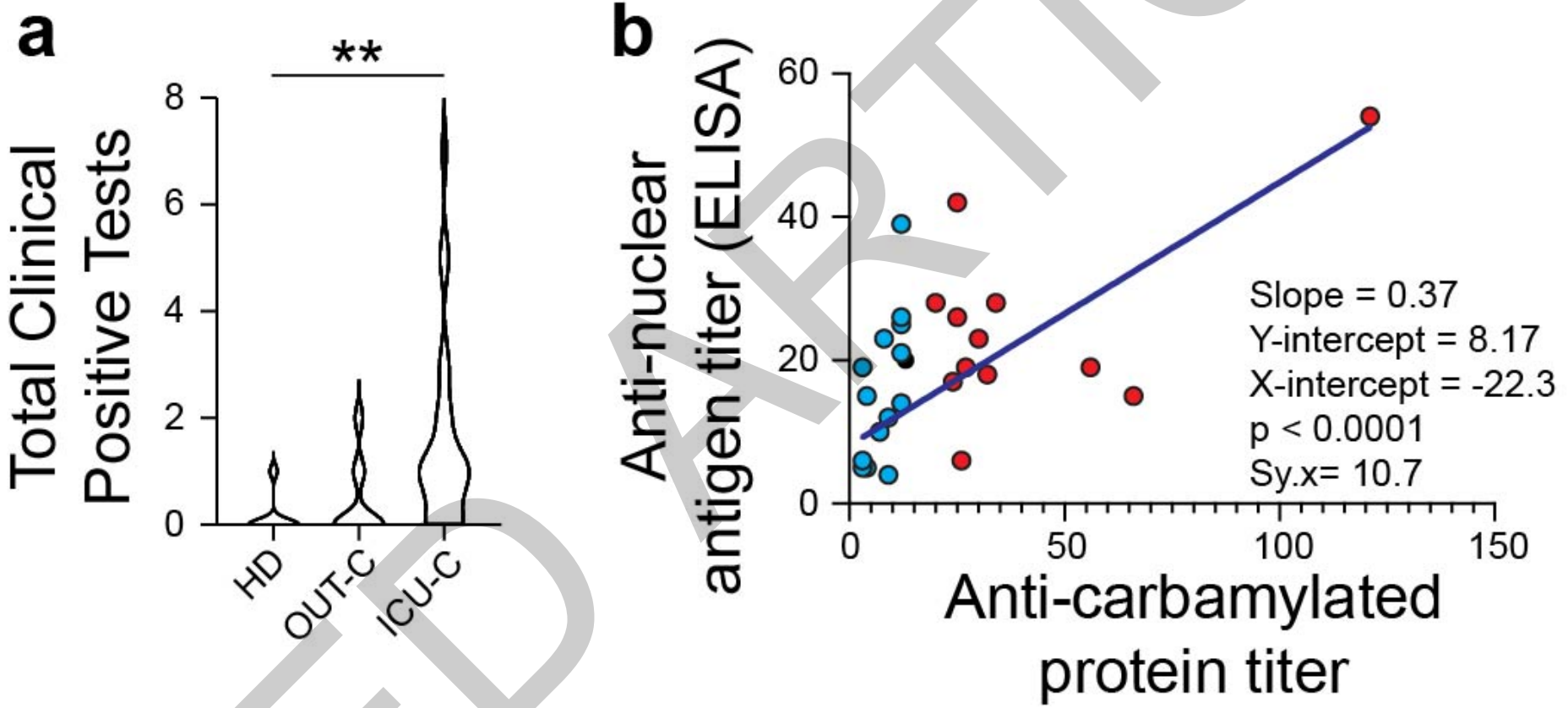

Extended data 6

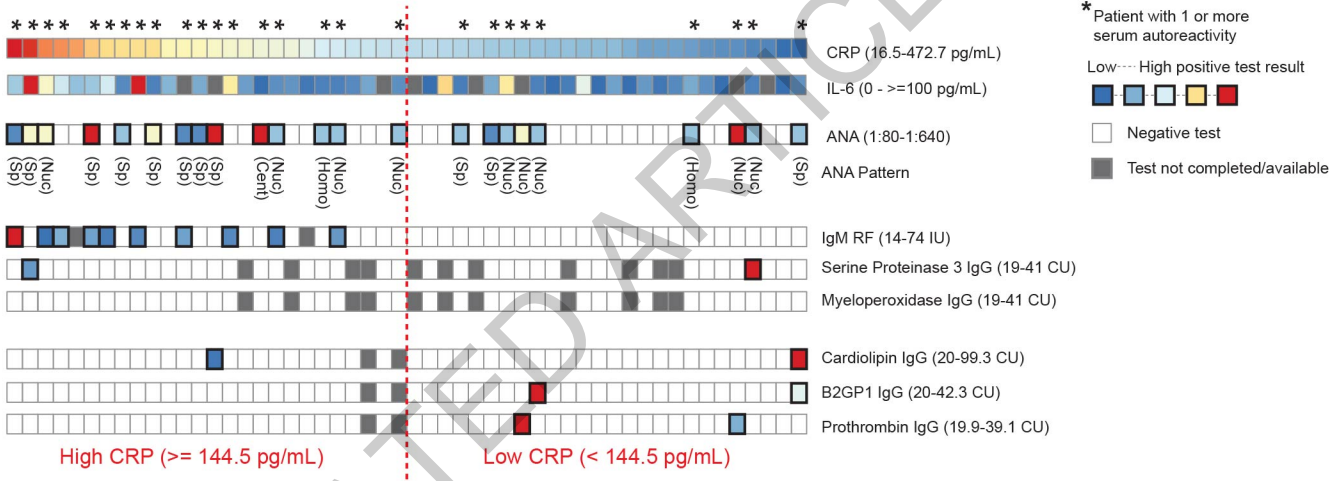

Extended data 7

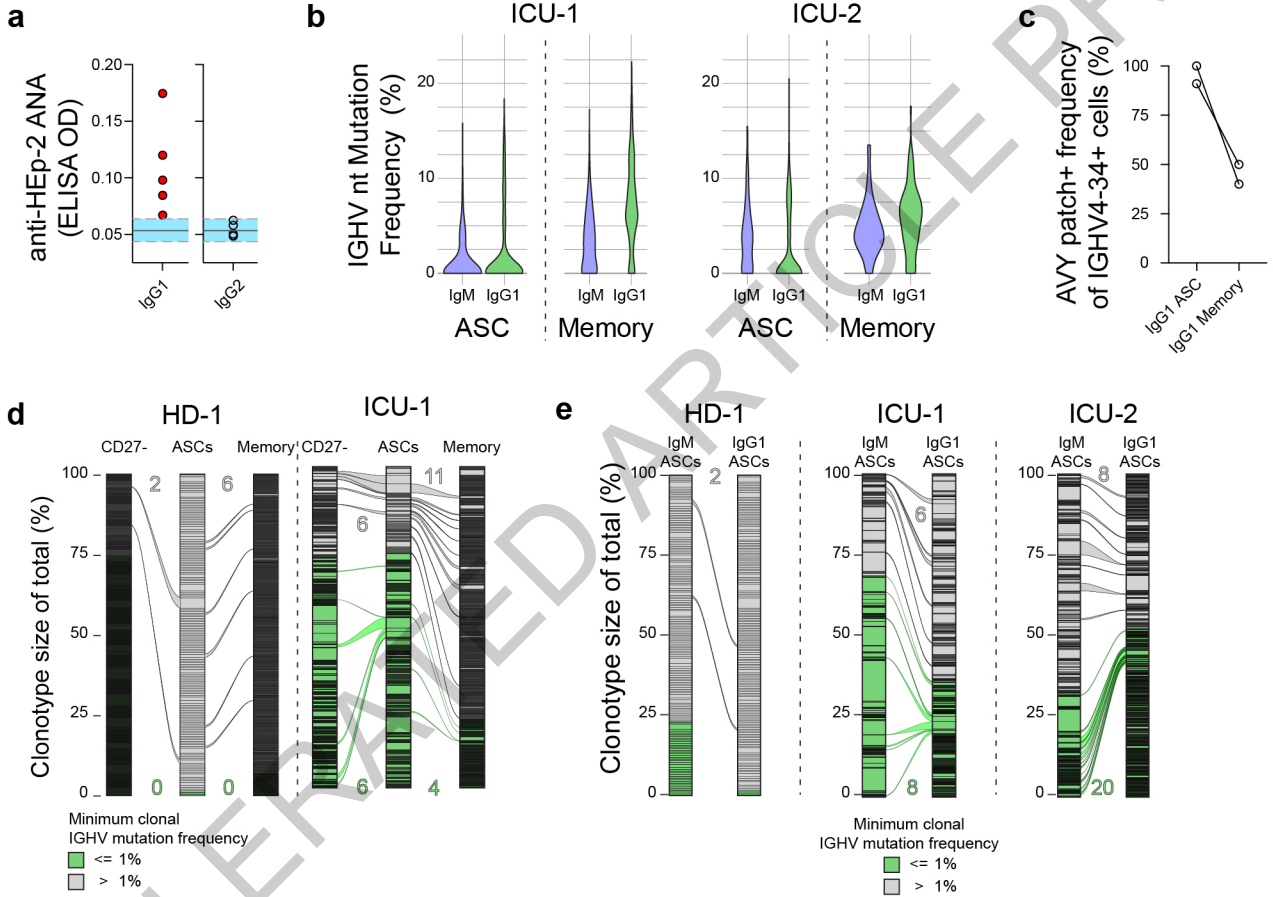

Extended data 8

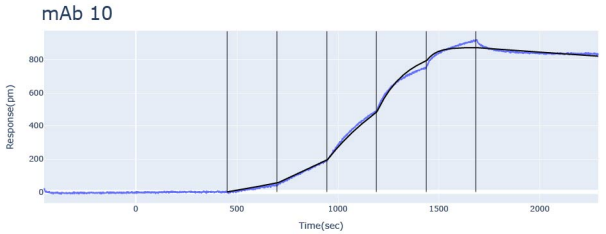

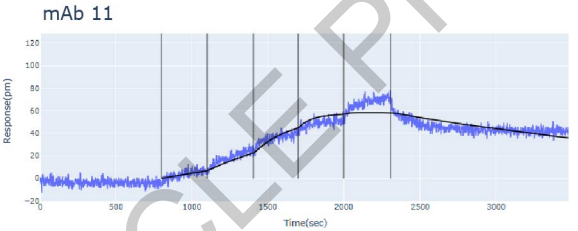

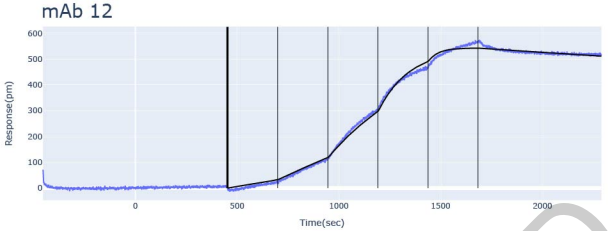

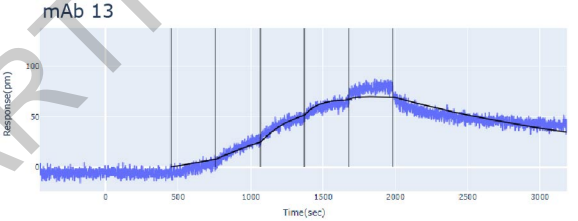

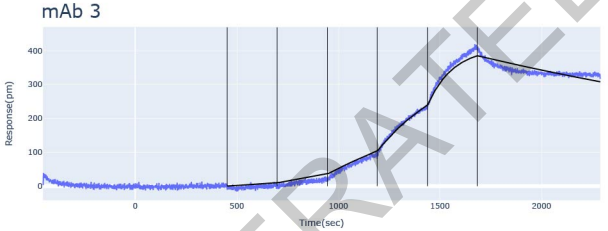

mAb ID	Target	ka (1/(M*s)	kd (1/s)	KD (M)
mAb 11	S2P	1.68E+05 (±2.57E+04)	4.59E-04 (±1.05E-04)	2.82E-09 (±1.00E-09)
mAb 13	S2P	2.61E+04 (±7.45E+03)	8.36E-04 (±2.25E-04)	3.27E-08 (±8.39E-09)
mAb 10	Nucleocapsid	1.18E+05 (±3.7E+04)	1.15E-04 (±2.52E-05)	9.93E-10 (±9.55E-11)
mAb 12	Nucleocapsid	1.50E+05 (±5.70E+04)	1.60E-04 (±7.34E-05)	1.12E-09 (±4.83E-10)
mAb 3	Nucleocapsid	4.32E+04 (±9.44E+03)	4.2E-04 (±9.97E-05)	1.00E-08 (±3.04E-09)

Extended data 9

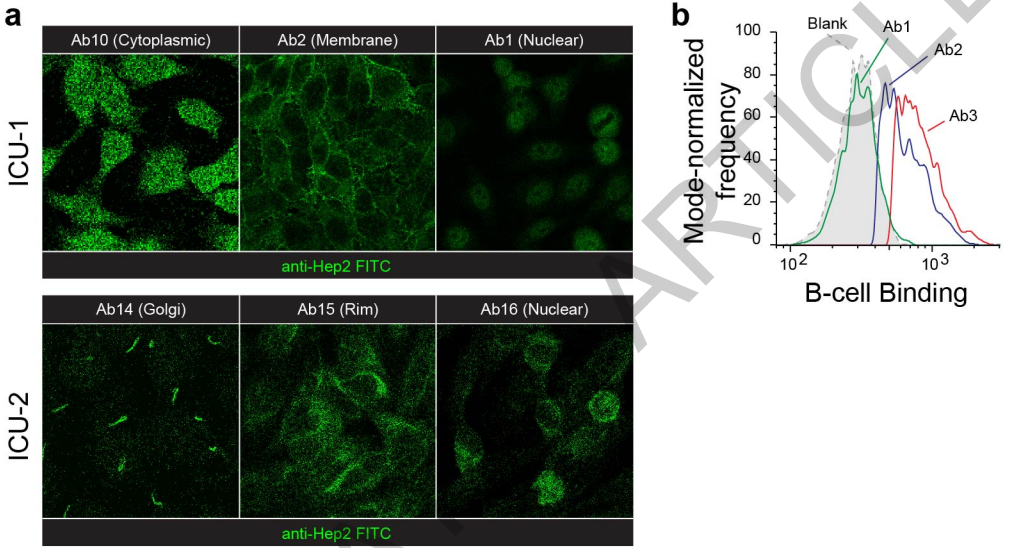

Extended data 10

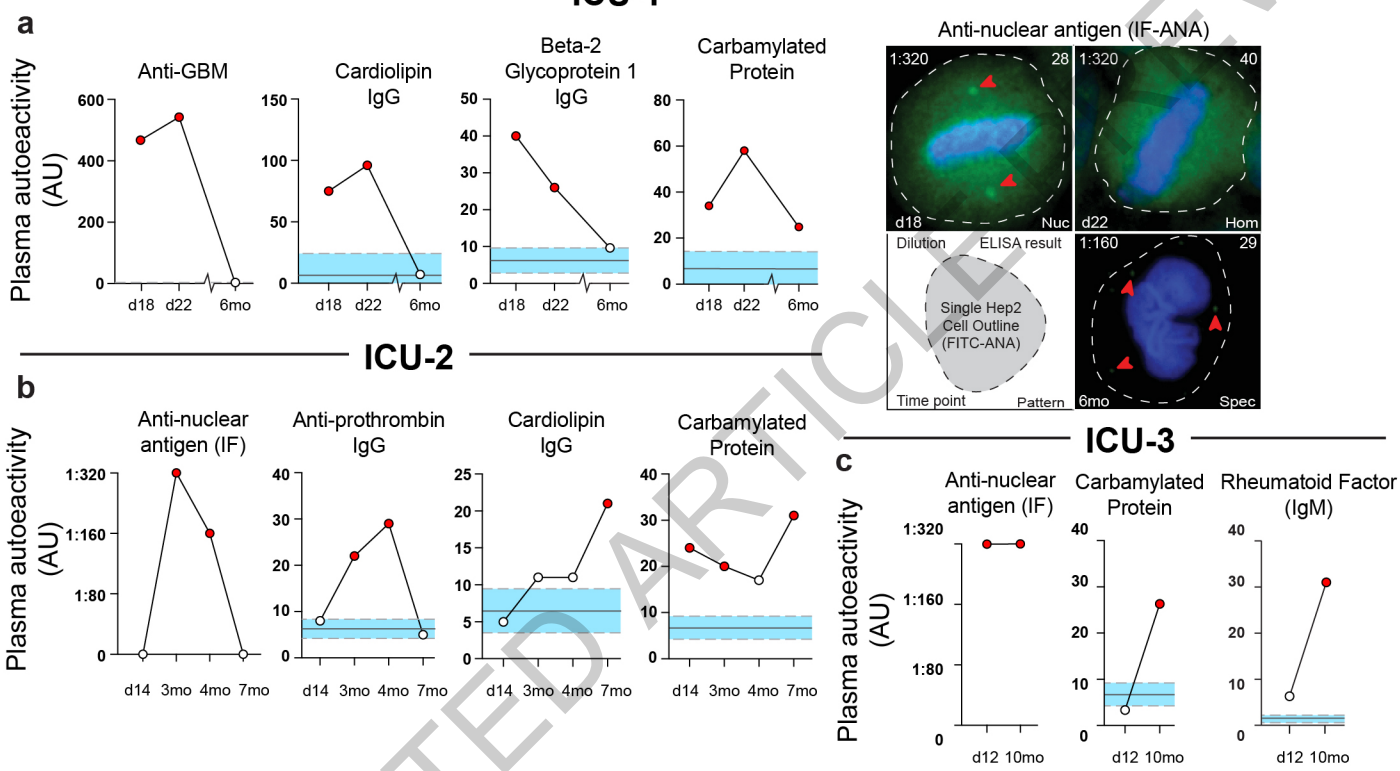

nature portfolio

Corresponding author(s): Dr. Ignacio Sanz

Last updated by author(s): 08/15/2022

Reporting Summary

Nature Portfolio wishes to improve the reproducibility of the work that we publish. This form provides structure for consistency and transparency in reporting. For further information on Nature Portfolio policies, see our Editorial Policies and the Editorial Policy Checklist.

Statistics

For all statistical analyses, confirm that the following items are present in the figure legend, table legend, main text, or Methods section.

n/a	Confirmed	
☐	☒	The exact sample size (*n*) for each experimental group/condition, given as a discrete number and unit of measurement
☐	☒	A statement on whether measurements were taken from distinct samples or whether the same sample was measured repeatedly
☐	☒	The statistical test(s) used AND whether they are one- or two-sided *Only common tests should be described solely by name; describe more complex techniques in the Methods section.*
☒	☐	A description of all covariates tested
☒	☐	A description of any assumptions or corrections, such as tests of normality and adjustment for multiple comparisons
☐	☒	A full description of the statistical parameters including central tendency (e.g. means) or other basic estimates (e.g. regression coefficient) AND variation (e.g. standard deviation) or associated estimates of uncertainty (e.g. confidence intervals)
☐	☒	For null hypothesis testing, the test statistic (e.g. *F*, *t*, *r*) with confidence intervals, effect sizes, degrees of freedom and *P* value noted *Give P values as exact values whenever suitable.*
☒	☐	For Bayesian analysis, information on the choice of priors and Markov chain Monte Carlo settings
☒	☐	For hierarchical and complex designs, identification of the appropriate level for tests and full reporting of outcomes
☐	☒	Estimates of effect sizes (e.g. Cohen's *d*, Pearson's *r*), indicating how they were calculated

Our web collection on statistics for biologists contains articles on many of the points above.

Software and code

Policy information about availability of computer code

Data collection	Patient data was collected using RedCAP data capture software. Flow cytometry data was collected on a Cytek Aurora flow cytometer using Cytek SpectroFlo software. Luminex data (including antigen specific data) was analyzed using a Luminex FLEXMAP 3D® instrument (Luminex; Austin, TX, USA) running xPonent 4.3 software. Repertoire data was sequenced by Novogene, and then processed through the 10x VDJ repertoire pipeline. Resulting sequences of high confidence were then mapped using IMGT's V-quest B cell receptor mapping software.
Data analysis	Computational analysis was carried out in R (v3.6.2; release 12 Dec 2019). Heat maps were generated using the pheatmap library (v1.0.12), with data pre-normalized (log-transformed z-scores calculated per feature) before plotting. Custom plotting, such as mutation frequency violin plots, was performed using the ggplot2 library for base analysis, and then post-processed in Adobe Illustrator. Alluvial plotting was performed using the ggalluvial package with post-processing in Adobe Illustrator. Clonotype connectivity analysis was carried out using the R-based 'vegan' package, and then visualized through 'pheatmap' before post-processing in Adobe Illustrator. Statistical analyses were performed directly in R, or in GraphPad Prism (v8.2.1). Analyses on the single cell VDJ annotated sequences were performed using the Immcantation tool suite (http://www.immcantation.org) version 4.1.0 pipeline in Docker. This suite contains SHazaM for statistical analysis of somatic hypermutation (SHM) patterns as described in (Gupta et al., 2015), and BASELINe (Bayesian estimation of Antigen-driven SELectIoN) for analysis of selection pressure as described in (Yaari et al., 2012). Visualizations were generated in R using the SHazaM package (version 1.0.2) and then post-processed in Adobe Illustrator.

For manuscripts utilizing custom algorithms or software that are central to the research but not yet described in published literature, software must be made available to editors and reviewers. We strongly encourage code deposition in a community repository (e.g. GitHub). See the Nature Portfolio guidelines for submitting code & software for further information.

Data

Policy information about availability of data

All manuscripts must include a data availability statement. This statement should provide the following information, where applicable:

- Accession codes, unique identifiers, or web links for publicly available datasets
- A description of any restrictions on data availability
- For clinical datasets or third party data, please ensure that the statement adheres to our policy

All FCM and sequencing data presented here are publicly available in alignment with current requirements for public disclosure before peer review. All FCM data presented and analyzed in this manuscript (Fig. 1) are publicly available in the FlowRepository at http://flowrepository.org/id/FR-FCM-Z2XF/.

Field-specific reporting

Please select the one below that is the best fit for your research. If you are not sure, read the appropriate sections before making your selection.

☐ Life sciences ☐ Behavioural & social sciences ☐ Ecological, evolutionary & environmental sciences

For a reference copy of the document with all sections, see nature.com/documents/nr-reporting-summary-flat.pdf

Life sciences study design

All studies must disclose on these points even when the disclosure is negative.

Sample size	*Describe how sample size was determined, detailing any statistical methods used to predetermine sample size OR if no sample-size calculation was performed, describe how sample sizes were chosen and provide a rationale for why these sample sizes are sufficient.*
Data exclusions	*Describe any data exclusions. If no data were excluded from the analyses, state so OR if data were excluded, describe the exclusions and the rationale behind them, indicating whether exclusion criteria were pre-established.*
Replication	*Describe the measures taken to verify the reproducibility of the experimental findings. If all attempts at replication were successful, confirm this OR if there are any findings that were not replicated or cannot be reproduced, note this and describe why.*
Randomization	*Describe how samples/organisms/participants were allocated into experimental groups. If allocation was not random, describe how covariates were controlled OR if this is not relevant to your study, explain why.*
Blinding	*Describe whether the investigators were blinded to group allocation during data collection and/or analysis. If blinding was not possible, describe why OR explain why blinding was not relevant to your study.*

Behavioural & social sciences study design

All studies must disclose on these points even when the disclosure is negative.

Study description	*Briefly describe the study type including whether data are quantitative, qualitative, or mixed-methods (e.g. qualitative cross-sectional, quantitative experimental, mixed-methods case study).*
Research sample	*State the research sample (e.g. Harvard university undergraduates, villagers in rural India) and provide relevant demographic information (e.g. age, sex) and indicate whether the sample is representative. Provide a rationale for the study sample chosen. For studies involving existing datasets, please describe the dataset and source.*
Sampling strategy	*Describe the sampling procedure (e.g. random, snowball, stratified, convenience). Describe the statistical methods that were used to predetermine sample size OR if no sample-size calculation was performed, describe how sample sizes were chosen and provide a rationale for why these sample sizes are sufficient. For qualitative data, please indicate whether data saturation was considered, and what criteria were used to decide that no further sampling was needed.*
Data collection	*Provide details about the data collection procedure, including the instruments or devices used to record the data (e.g. pen and paper, computer, eye tracker, video or audio equipment) whether anyone was present besides the participant(s) and the researcher, and whether the researcher was blind to experimental condition and/or the study hypothesis during data collection.*
Timing	*Indicate the start and stop dates of data collection. If there is a gap between collection periods, state the dates for each sample cohort.*
Data exclusions	*If no data were excluded from the analyses, state so OR if data were excluded, provide the exact number of exclusions and the rationale behind them, indicating whether exclusion criteria were pre-established.*
Non-participation	*State how many participants dropped out/declined participation and the reason(s) given OR provide response rate OR state that no participants dropped out/declined participation.*

Randomization

If participants were not allocated into experimental groups, state so OR describe how participants were allocated to groups, and if allocation was not random, describe how covariates were controlled.

Ecological, evolutionary & environmental sciences study design

All studies must disclose on these points even when the disclosure is negative.

Study description

Briefly describe the study. For quantitative data include treatment factors and interactions, design structure (e.g. factorial, nested, hierarchical), nature and number of experimental units and replicates.

Research sample

Describe the research sample (e.g. a group of tagged Passer domesticus, all Stenocereus thurberi within Organ Pipe Cactus National Monument), and provide a rationale for the sample choice. When relevant, describe the organism taxa, source, sex, age range and any manipulations. State what population the sample is meant to represent when applicable. For studies involving existing datasets, describe the data and its source.

Sampling strategy

Note the sampling procedure. Describe the statistical methods that were used to predetermine sample size OR if no sample-size calculation was performed, describe how sample sizes were chosen and provide a rationale for why these sample sizes are sufficient.

Data collection

Describe the data collection procedure, including who recorded the data and how.

Timing and spatial scale

Indicate the start and stop dates of data collection, noting the frequency and periodicity of sampling and providing a rationale for these choices. If there is a gap between collection periods, state the dates for each sample cohort. Specify the spatial scale from which the data are taken

Data exclusions

If no data were excluded from the analyses, state so OR if data were excluded, describe the exclusions and the rationale behind them, indicating whether exclusion criteria were pre-established.

Reproducibility

Describe the measures taken to verify the reproducibility of experimental findings. For each experiment, note whether any attempts to repeat the experiment failed OR state that all attempts to repeat the experiment were successful.

Randomization

Describe how samples/organisms/participants were allocated into groups. If allocation was not random, describe how covariates were controlled. If this is not relevant to your study, explain why.

Blinding

Describe the extent of blinding used during data acquisition and analysis. If blinding was not possible, describe why OR explain why blinding was not relevant to your study.

Did the study involve field work? ☐ Yes ☐ No

Field work, collection and transport

Field conditions

Describe the study conditions for field work, providing relevant parameters (e.g. temperature, rainfall).

Location

State the location of the sampling or experiment, providing relevant parameters (e.g. latitude and longitude, elevation, water depth).

Access & import/export

Describe the efforts you have made to access habitats and to collect and import/export your samples in a responsible manner and in compliance with local, national and international laws, noting any permits that were obtained (give the name of the issuing authority, the date of issue, and any identifying information).

Disturbance

Describe any disturbance caused by the study and how it was minimized.

Reporting for specific materials, systems and methods

We require information from authors about some types of materials, experimental systems and methods used in many studies. Here, indicate whether each material, system or method listed is relevant to your study. If you are not sure if a list item applies to your research, read the appropriate section before selecting a response.

Materials & experimental systems

n/a	Involved in the study
☐	☒ Antibodies
☒	☐ Eukaryotic cell lines
☒	☐ Palaeontology and archaeology
☒	☐ Animals and other organisms
☐	☒ Human research participants
☒	☐ Clinical data
☒	☐ Dual use research of concern

Methods

n/a	Involved in the study
☐	☐ ChIP-seq
☐	☒ Flow cytometry
☐	☐ MRI-based neuroimaging

Antibodies

Antibodies used

Target; Fluorophore; Panel; Clone; Vendor; Cat#; Dilution (ul/100ul)
CD62L BV480 v1, v2 DREG-56 BD 566174 5 ul
CD86 PerCP-Cy5.5 v1, v2 IT2.2 Biolegend 305419 5 ul
CD27 BV750 v1, v2, ICS O323 Biolegend 302849 2.5 ul
CD19 BV570 v1, v2, ICS HIB19 Biolegend 302235 2.5 ul
CD45 Spark NIR 685 v2 2D1 Biolegend 368552 1.25 ul
CD1c BV510 v2 L161 Biolegend 331534 1.25 ul
IgM BV711 v1, v2, ICS MHM-88 Biolegend 314539 1.25 ul
CXCR3 A647 v1, v2, ICS G025H7 Biolegend 353711 1.25 ul
CXCR4 PerCP-e710 v1, v2 12G5 eBioscience 46-9999-41 1.25 ul
CCR7 A488 v1 G043H7 Biolegend 353205 1.25 ul
CD24 PerCP v1, v2, ICS ML5 Biolegend 311113 1.25 ul
CD3 BUV 805 v1, v2, ICS UCHT1 BD 612896 0.6 ul
CD11c APC-Fire750 v1, v2, ICS S-HCL-3 Biolegend 371509 0.6 ul
CD138 APC-R700 v1, v2 MI15 BD 566051 0.6 ul
HLA-DR BV650 v1, v2 L243 Biolegend 307649 0.6 ul
CD95 BV785 v1, v2 DX2 Biolegend 305645 0.6 ul
CD14 BUV805 v1, v2 M5E2 BD 612902 0.6 ul
CD23 APC v2 EBVCS-5 Biolegend 338514 0.3 ul
CD69 BUV 737 v1, v2 FN50 BD 612817 0.3 ul
IgD BV605 v1, v2, ICS IA6-2 Biolegend 348231 0.3 ul
CD21 PE-Dazzle594 v1, v2, ICS Bu32 Biolegend 354921 0.3 ul
CD38 BB515 v1, v2, ICS HIT2 BD 564499 0.3 ul
CXCR5 PE v1, v2, ICS J252D4 Biolegend 356903 0.3 ul
CD40 A532 v1, v2 5C3 Novus NBP1-43416AF523 0.3 ul
PD-1 PE-Cy7 v1, v2 EH12.2H7 Biolegend 239917 0.3 ul
IgG BV421 v1, v2 M1310G05 Biolegend 410703 0.15 ul
CD10 PE-Cy5 v1, v2 HI10a Biolegend 312205 0.15 ul
CD25 e450 v1 BC96 eBioscience 48-0259-41 5 ul
CD1d BV510 v1 51.1 Biolegend 350313 2.5 ul
ICOS-L APC v1 2D3 Biolegend 309407 5 ul
B220 Spark NIR 685 v1 RA3-6B2 Biolegend 103268 2.5 ul
T-bet APC ICS 4B10 Biolegend 644814 1.25 ul
Viability Zombie NIR v1,2 NA Biolegend 423106 0.2 ul

Validation

All antibodies have been validated by the manufacturer for use in targeting human proteins as indicated above.

Human research participants

Policy information about studies involving human research participants

Population characteristics

Population characteristics are fully described in Supplementary table 1 of the manuscript.

Recruitment

Written informed consent was obtained from all participants or, if they were unable to provide informed consent, obtained from designated healthcare surrogates. Healthy donors (n = 36) were recruited using promotional materials approved by the Emory University Institutional Review Board. Subjects with COVID-19 (n = 19) were recruited from Emory University Hospital, Emory University Hospital Midtown and Emory St. Joseph's Hospital, all in Atlanta, GA, USA. All non-healthy donor subjects were diagnosed with COVID-19 by PCR amplification of SARS-CoV-2 viral RNA obtained from nasopharyngeal or oropharyngeal swabs. Subjects with COVID-19 were included in the study if they were 18 to 80 years of age, not immunocompromised, and had not been given oral or intravenous corticosteroids within the preceding 14 days.

Ethics oversight

All research was approved by the Emory University Institutional Review Board (Emory IRB numbers IRB00058507, IRB00057983, and IRB00058271) and was performed in accordance with all relevant guidelines and regulations.

Note that full information on the approval of the study protocol must also be provided in the manuscript.

ChIP-seq

Data deposition

☐ Confirm that both raw and final processed data have been deposited in a public database such as GEO.

☐ Confirm that you have deposited or provided access to graph files (e.g. BED files) for the called peaks.

Data access links
May remain private before publication.

For "Initial submission" or "Revised version" documents, provide reviewer access links. For your "Final submission" document, provide a link to the deposited data.

Files in database submission

Provide a list of all files available in the database submission.

Genome browser session (e.g. UCSC)	*Provide a link to an anonymized genome browser session for "Initial submission" and "Revised version" documents only, to enable peer review. Write "no longer applicable" for "Final submission" documents.*

Methodology

Replicates	*Describe the experimental replicates, specifying number, type and replicate agreement.*
Sequencing depth	*Describe the sequencing depth for each experiment, providing the total number of reads, uniquely mapped reads, length of reads and whether they were paired- or single-end.*
Antibodies	*Describe the antibodies used for the ChIP-seq experiments; as applicable, provide supplier name, catalog number, clone name, and lot number.*
Peak calling parameters	*Specify the command line program and parameters used for read mapping and peak calling, including the ChIP, control and index files used.*
Data quality	*Describe the methods used to ensure data quality in full detail, including how many peaks are at FDR 5% and above 5-fold enrichment.*
Software	*Describe the software used to collect and analyze the ChIP-seq data. For custom code that has been deposited into a community repository, provide accession details.*

Flow Cytometry

Plots

Confirm that:

☒ The axis labels state the marker and fluorochrome used (e.g. CD4-FITC).

☒ The axis scales are clearly visible. Include numbers along axes only for bottom left plot of group (a 'group' is an analysis of identical markers).

☒ All plots are contour plots with outliers or pseudocolor plots.

☒ A numerical value for number of cells or percentage (with statistics) is provided.

Methodology

Sample preparation	Peripheral blood samples were collected in heparin sodium tubes and processed within 6 hours of collection. PBMCs were isolated by density gradient centrifugation at 1000 x g for 10 minutes. Aliquots from the plasma layer were collected and stored at -80C until use. PBMCs were washed 2 times with RPMI at 500 x g for 5 minutes.
Instrument	Cells were analyzed on a Cytek Aurora flow cytometer (V3; 16V-14B-10YG-8R)
Software	Cells were analyzed on a Cytek Aurora flow cytometer using Cytek SpectroFlo software. Up to 3 x 106 cells were analyzed using FlowJo v10 (Treestar) software.
Cell population abundance	NA
Gating strategy	Gating strategy is provided in supplementary figure 1.

☒ Tick this box to confirm that a figure exemplifying the gating strategy is provided in the Supplementary Information.

Magnetic resonance imaging

Experimental design

Design type	*Indicate task or resting state; event-related or block design.*
Design specifications	*Specify the number of blocks, trials or experimental units per session and/or subject, and specify the length of each trial or block (if trials are blocked) and interval between trials.*
Behavioral performance measures	*State number and/or type of variables recorded (e.g. correct button press, response time) and what statistics were used to establish that the subjects were performing the task as expected (e.g. mean, range, and/or standard deviation across subjects).*

Acquisition

Imaging type(s) — *Specify: functional, structural, diffusion, perfusion.*

Field strength — *Specify in Tesla*

Sequence & imaging parameters — *Specify the pulse sequence type (gradient echo, spin echo, etc.), imaging type (EPI, spiral, etc.), field of view, matrix size, slice thickness, orientation and TE/TR/flip angle.*

Area of acquisition — *State whether a whole brain scan was used OR define the area of acquisition, describing how the region was determined.*

Diffusion MRI ☐ Used ☐ Not used

Preprocessing

Preprocessing software — *Provide detail on software version and revision number and on specific parameters (model/functions, brain extraction, segmentation, smoothing kernel size, etc.).*

Normalization — *If data were normalized/standardized, describe the approach(es): specify linear or non-linear and define image types used for transformation OR indicate that data were not normalized and explain rationale for lack of normalization.*

Normalization template — *Describe the template used for normalization/transformation, specifying subject space or group standardized space (e.g. original Talairach, MNI305, ICBM152) OR indicate that the data were not normalized.*

Noise and artifact removal — *Describe your procedure(s) for artifact and structured noise removal, specifying motion parameters, tissue signals and physiological signals (heart rate, respiration).*

Volume censoring — *Define your software and/or method and criteria for volume censoring, and state the extent of such censoring.*

Statistical modeling & inference

Model type and settings — *Specify type (mass univariate, multivariate, RSA, predictive, etc.) and describe essential details of the model at the first and second levels (e.g. fixed, random or mixed effects; drift or auto-correlation).*

Effect(s) tested — *Define precise effect in terms of the task or stimulus conditions instead of psychological concepts and indicate whether ANOVA or factorial designs were used.*

Specify type of analysis: ☐ Whole brain ☐ ROI-based ☐ Both

Statistic type for inference (See Eklund et al. 2016) — *Specify voxel-wise or cluster-wise and report all relevant parameters for cluster-wise methods.*

Correction — *Describe the type of correction and how it is obtained for multiple comparisons (e.g. FWE, FDR, permutation or Monte Carlo).*

Models & analysis

n/a	Involved in the study
☐	☐ Functional and/or effective connectivity
☐	☐ Graph analysis
☐	☐ Multivariate modeling or predictive analysis

Functional and/or effective connectivity — *Report the measures of dependence used and the model details (e.g. Pearson correlation, partial correlation, mutual information).*

Graph analysis — *Report the dependent variable and connectivity measure, specifying weighted graph or binarized graph, subject- or group-level, and the global and/or node summaries used (e.g. clustering coefficient, efficiency, etc.).*

Multivariate modeling and predictive analysis — *Specify independent variables, features extraction and dimension reduction, model, training and evaluation metrics.*